UNIVERSIDAD DE CANTABRIA

Departamento de Ciencias y Técnicas del Agua y del Medio Ambiente

Numerical modeling of the global wave climate variability and associated environmental and technological risks

---

A Doctoral Thesis by: Borja González Reguero

Advisors: Iñigo J. Losada and Fernando J. Méndez

Santander, December, 2012

Chapter 4

Technological Risks

"However beautiful the strategy, you should occasionally look at the results"

Winston Churchill

4.1 Introduction

To date, design and operation of ocean and coastal infrastructures rely on historical climate information. Time history series of observation and for numerical reanalysis of the relevant variables have been usually treated in engineering using statistical tools based on the assumption of stationarity. However, the expected life cycle of any coastal or offshore structure, reaching form the the project phase to the decommission phase usually includes several decades. Moreover, just the operation phase or useful life is expected to be of well over 20 years at least.

In the context and time scales of sea level rise, inter-annual variability and long-term trends of marine environmental variables evidenced by an important body of scientific contribution during the last decade, neglecting the non-stationarity of these processes over the life cycle of coastal and offshore facilities will end up in an increasing technological risk that may end in reliability losses, operation underperformance and underestimated costs.

Needless to say that wave farms are not an exception. Designed and optimized to operate under a given limited range of available wave power, on site and for specific survivability conditions, estimated from specific combinations of mean extreme wave heights, wave periods and water levels; their life cycle is surely affected by marine climate variability. Consequently, mitigation of technological risk in offshore wave farms demands the assessment of environmental conditions variability as a driver of risk.

The present chapter presents a set of methods and criteria for providing an assessment of the technological risk at a global scale for three generic concepts of floating Wave Energy Converters (WECs).

The chapter is organized as follows. The risk assessment approach, followed in this work,

starts in Section 4.2 devoted to the evaluation of the variability of the global wave energy resources available and the analysis of its variability at different time scales relevant for the life-cycle of wave farms. In Section 4.3 the technological risk is explained in detail considering how changes in the resources and extreme conditions will affect the performance of selected WEC technologies. The spatial variation at a global scale of some relevant indicators is calculated and represented in global maps. The chapter closes with a set of relevant conclusions.

4.2 Global wave energy resource assessment

4.2.1 Introduction

Solar energy is the most abundant permanent energy source an is available for indirect use from the global ocean. Within renewable energies, characterized by being naturally replenished, sustainable, and only marginally alter the carbon balance in the atmosphere ([Angelis-Dimakis et al., 2010]), ocean energy can produce thermal (from sun´s heat) and mechanical energy (from tides and wind-waves). When studying ocean energy not only tidal/marine current energy must be considered but also wave energy may play an important role towards sustainability. This type of energy is expected to be economically competitive, by the development of new designs and technical improvements ([Falnes and Lovseth, 1991, Thorpe, 1992, Thorpe, 1999]).

[Jacobson, 2009] reviewed and ranked major proposed energy-related solutions to global warming, air pollution and energy security while considering other ecological and socioeconomic impacts. It ranked wave energy option into tier 2, labeled as recommended and providing significant benefits. On their overall ranking wave energy falls into position 7th out of the twelve energy options into consideration.

Nowadays, wave energy can be regarded to be at its pre-commercial phase and hence much work is being carried out on the evaluation of the wave energy potential and the detailed characterization of this energy source. On a global perspective, several works evaluate global wave energy based on satellite altimeter or wave reanalysis data ([Krogstad and Barstow, 1999, Pontes et al., 2002, Barstow et al., 2008, Cornett, 2008, Mork et al., 2010]). In this work, the use of both types of datasets is proposed: a 1-hour wave reanalysis database covering a period of 61 years and satellite altimeter measurements embedded through a correction of the simulated wave fields. Therefore, a methodology is also developed to obtain reliable estimates of the spatial and temporal variability of global wave energy resources covering the last six decades.

Because ocean wave energy is intimately related with wave climate, the random nature of waves makes it necessary an adequate assessment of the temporal variability of wave energy. As remarked by [Falcao, 2010] and [Mackay et al., 2010], the main disadvantage of wave power is the large random variability in different time scales, distinguishing: wave to wave, sea states, month, seasonal and inter-annual variation. Wave Energy Converters (WECs) design and site-specific optimization requires not only mean values of characteristic variables over a given time period, but also their expected range of variation. Accounting for the random nature of waves, the mean annual value of wave energy is not a complete descriptor of the resource because it

does not capture its variability.

[Cornett, 2008] studied the variability of the resource for a 10-year period. In a lower time scale, [Myrhaug et al., 2009a, Myrhaug et al., 2009b] and [Izadparast and Niedzwecki, 2011] studied the probability distribution function of wave power in a sea-state scale. Moreover, wave power can vary from on a monthly basis and, similarly, from year to year (i.e. climate inter-annual variability). One cause of this variability is the temporal variable influence of patterns in the characteristic wave climate, known as climatic variability, whose effects act over several years cycles. Investigation has turned to find connections between wave climate parameters and different climate indices (e.g., [Wang and Swail, 2001, Woolf and Challenor, 2002, Gulev and Grigorieva, 2004, Lionello and Sanna, 2005, Menendez et al., 2008, Izaguirre et al., 2011]).

Those findings indicate that climate patterns, of which North Atlantic Oscillation or Southern Annular Mode are significant examples, may affect wave climate over several years cycles and, consequently, modify the wave energy power. [Harrison and Wallace, 2005] stressed that the potential of wave energy is related to the variations in the climatic conditions that would influence long-term resource. On a regional basis, current research is trying to cover the gap between seasonal and decadal oscillations, see for example [Ching-Piao et al., 2012] and the relationship between El-Niño phenomenon and the wave energy for northeast coast of Taiwan.

Besides, a big controversy on the available resource of wave energy still exists in recent literature. Only [Mork et al., 2010] estimated the available theoretical wave power along offshore worldwide coastline and on a regional basis. In this work the theoretical wave power potential is assessed taking into consideration the wave energy direction and showing that wave energy potential is lower than current estimations due to directional restrictions.

This section deals with the assessment of the global wave energy potential and its variability at different time scales. The link between wave power and natural climatic variability is also studied. Section 4.2.2 describes the general methodology to evaluate the wave energy resource, accounting for the data, the comparison with measurements and the theoretical background. It finally focuses on the assessment of the global wave energy resource including the evaluation of the mean wave energy resource, the theoretical potential and a discussion on technical availability. Section 4.2.3 addresses the temporal variability of the resources, covering from annual to inter-annual and long-term scales and also accounts for the mean contribution of several climate patterns to global wave power. Overall conclusions of this part of the work are included in the final section of the chapter, specifically devoted to that purpose.

4.2.2 Global wave energy resources

4.2.2.1 Methodology

This study relies on a global framework that can be applied to different spatial scales. It combines different data bases and methodologies to obtain wave power statistics. The framework includes the following steps (see diagram in Figure 4.1): (1) generation of a wave reanalysis data base, (2) calibration with altimeter data, (3) validation with buoy data, and, finally, (4)

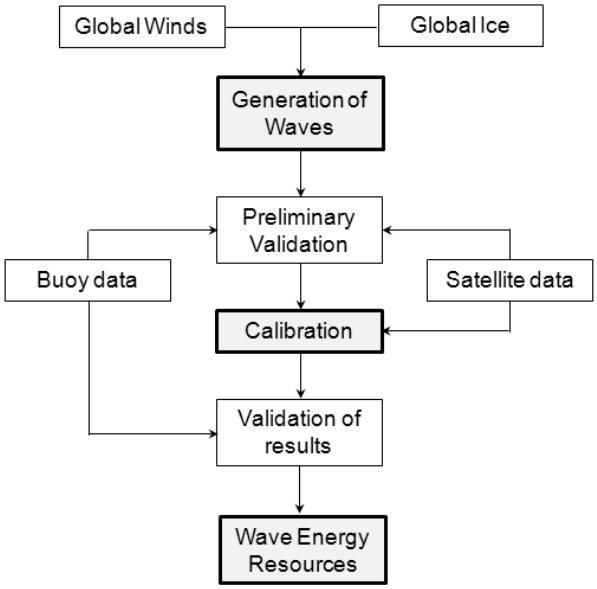

Figure 4.1: Diagram of the methodology to evaluate the offshore wave energy resources potential

assessment of the wave energy resources at deep water and analysis of its variability at a global scale.

The first step in the analysis is the generation of a global wind-waves database with a long enough temporal coverage. This dataset must be statistically homogenous with satellite altimeter observations. This characteristic is achieved by assimilating altimeter measurements in the simulations through a final correction for the wave heights so that the magnitude of the resources and its spatial and temporal variability can be adequately modeled.

4.2.2.2 Theoretical background

The energy flux or wave power (P) in a regular wave per unit width can be obtained as [Dean and Dalrymple, 1991]:

$$P = \frac{1}{8}\rho g H^2 c_g \tag{4.1}$$

where ρ is the water density, H is the wave height and c_g is the group velocity that can be obtained from:

$$c_g = \frac{1}{2}(1 + \frac{2kh}{\sinh(2kh)})\frac{L}{T} \tag{4.2}$$

where L is the wave length, k is the wave number $(2\pi/L)$, h is the water depth and T is the period. L and T are related through the known dispersion equation:

$$(\frac{2\pi}{T})^2 = gk\tanh(kh) \tag{4.3}$$

However, for irregular waves, the wave power has to be obtained from the spectral density function, $S(f,\theta)$, where f represents the frequency and θ the direction of waves, as:

$$P = \rho g \int\int c_g(f,h)\cdot S(f,\theta)dfd\theta \tag{4.4}$$

Sea-states of irregular waves are usually described by certain variables which characterize the spectral shape. One of them is the standard deviation of the surface elevation, H_{m0}, computed from the integral of the spectral density or order-zero moment, m_0, as:

$$H_{m0} = 4.004\cdot\sqrt{m_0} \tag{4.5}$$

For swell dominated sea states, the former parameter can be associated to the mean wave height (trough to crest) of the highest third of the waves in a sea-state, which is named as significant wave height and denoted by H_s. Other variables defining a sea-state are the peak or mean periods, T_{02} or T_{01}. Accordingly, the wave power for a irregular sea-state can be obtained from wave spectral parameters from the following expression:

$$P = \frac{\rho g^2}{64\pi}T_e H_s^2 \tag{4.6}$$

where T_e is known as the energy period, rarely specified but that can be estimated from the spectral shape and other parameters. For the case of the mean period, T_{01}, it can be obtained as:

$$T_e = \frac{m_{-1}}{m_0} = \alpha T_{01} \tag{4.7}$$

In this work, we use the mean wave period (T_{01}) which for a peak enhancement mean factor of 3.3 in a JONSWAP spectrum relates with T_e through a coefficient of $\alpha = 0.538$.

Strictly speaking, the assumption of a constant spectral shape introduces some uncertainty into the wave power estimates, but can be neglected considering that: (1) the error in the value of α is of an order lower than the values of T_{01} and H_s and (2) the errors in the period estimation

are less significant than those in wave heights since wave power relates to the square of the wave height. For this last reason a correct modeling of the significant wave heights is of utmost importance for global wave energy assessment.

The former equations determine the mean energy flux that crosses a cylinder of 1 m of diameter and the water column height, as sketched in Figure 4.2. Thereby, wave power is usually expressed in kw/m of wave front for evaluation purposes. In this work, wave parameters were computed from 1948 onwards obtaining hourly time series of wave power globally to be subjected to further analysis.

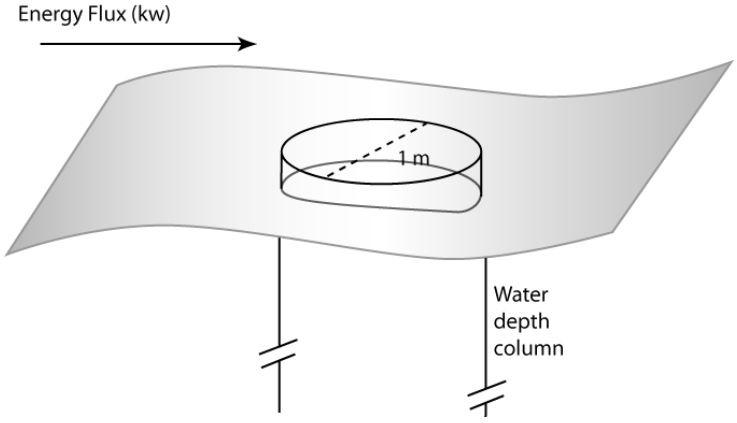

Figure 4.2: Wave Power calculation concept.

4.2.2.3 Data and validation of wave energy results

Lacking direct measurements with enough spatial and temporal coverage, wave reanalysis techniques are usually employed based on wind speeds and ice cover fields. In this study, a 61-year global wave reanalysis (GOW) is employed (see Chapter 2). The dataset provides hourly time series of wave parameters from 1948 up to 2008. This wave reanalysis has been generated using the model WaveWatchIII (WW3; [Tolman, 2002a, Tolman, 2002b]) and the NCEP/NCAR 6-h ice coverage and wind fields as input forcing. The spatial resolution in the open ocean is 1°x1.5° (latitude x longitude).

As seen in Chapter 2, the final dataset is a result of numerical modeling and several corrections with altimeter data. To judge the effect of the correction on wave power statistics, Figure 4.3 depicts the variation in the global mean wave power after applying the corrections, showing the absolute magnitude of mean wave power change (panel a) and the percentage of change with respect to the annual mean value (panel b). According to the differences obtained after the calibration, in the Northern Hemisphere (NH) there is a positive correction of about 10 kw/m in the North-West Atlantic, smaller in the North-West Pacific at the latitude of Japan and a decrease of the same order of magnitude in the North of Europe. On the contrary, in the Southern Hemisphere (SH) the effect of the correction is a general decrease in the estimation of -10kw/m at high latitudes, although there is also a positive correction at southern Africa. The largest corrections affect the coastal areas and semi-enclosed basins in relative terms (with respect to

unamended wave power conditions). It also corrects island shadowing due to an insufficient spatial resolution.

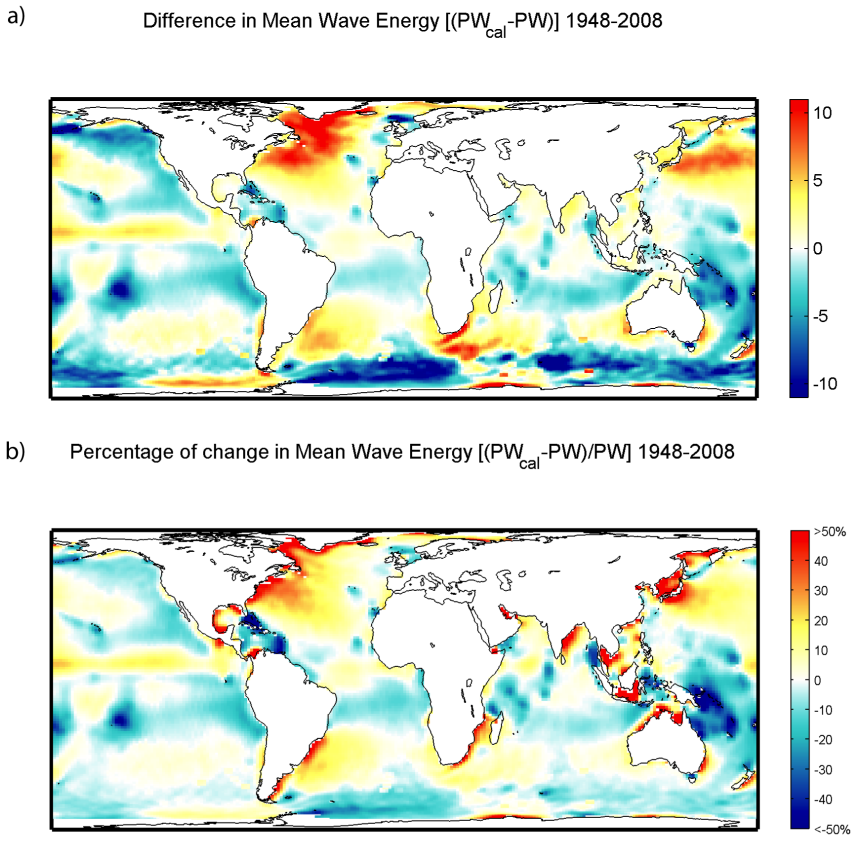

Figure 4.3: Changes in Mean Wave Power after the calibration of wave heights with altimeter observations, expressed in absolute magnitude (kw/m) (a) and in relative terms (%) (b)

In order to strengthen the quality of the correction of the numerical database a comparison of corrected numerical wave power vs. wave power obtained from wave buoys is carried out at several locations prior to any further analysis. Figure 4.4 shows the validation of the wave power at the North and South Atlantic and the North and Mid Pacific buoys, located in the Caribbean (CAR-41041, -46°E, 14.36°N, NOAA), North Pacific (ALA-46003, 154.98°E, 52.70°N, NOAA), Hawaii (HW-51001, -162.21°E, 23.43°N, NOAA) and North Atlantic (Silleiro, -9.39°E, 42.13°N, OPPE). These plots compare the monthly means and the annual mean wave power obtained from the buoy measurements and from the calibrated reanalysis data. The comparison reflects a fine agreement at both time scales. These results further support the assumption that the calibrated reanalysis database represents appropriately not only the mean wave power value, but also the mean monthly behavior.

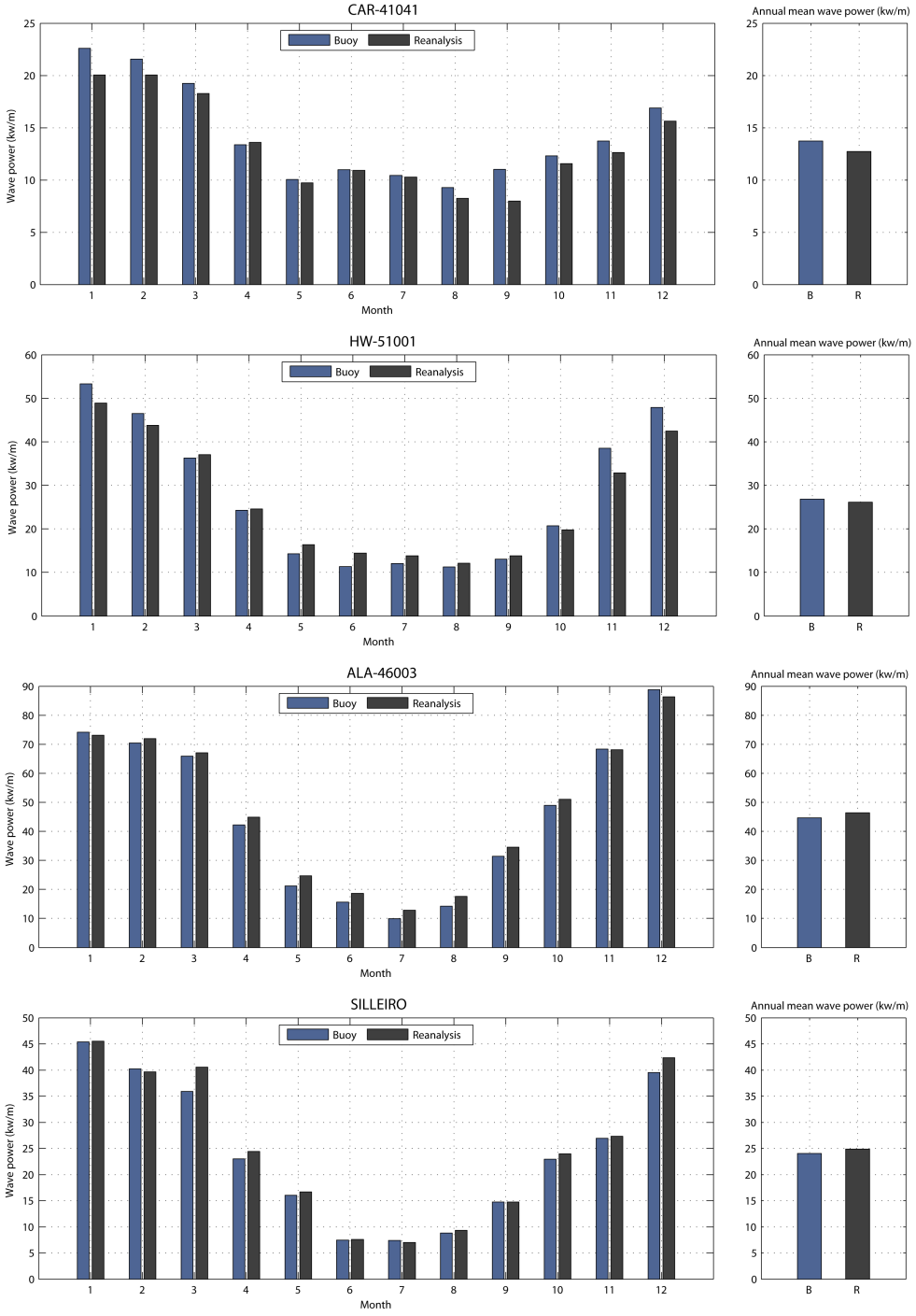

Figure 4.4: Comparison of instrumental buoy data (blue) and numerical results (gray) monthly mean wave power (left panels) and annual mean wave power (right panels). Data expressed in kw/m of wave front.

4.2.2.4 Theoretical available wave energy resources

Figure 4.5 shows the spatial pattern of the mean annual wave power from 1948 to 2008. Making a rough comparison between the NH and the SH, it seems clear that wave energy resources are larger in the SH. Largest values of the resources can be found in the South-Indian Ocean, with values of approximately 120 kw/m. Besides, values greater than 90 kw/m are found in the South Pacific. Regarding the NH, the highest values are found in the North-Atlantic between the 40 and 60°N, with values between 80 and 90 kw/m but gradually decreasing to 20 kw/m at approximately 20°N. The North American west coast is exposed to energy figures varying from 20 to 60 kw/m increasing in latitude. These areas are associated with the storm tracks in the SH and NH that come from the generation areas at high latitudes in both hemispheres ([Young, 1999]). This general pattern is in agreement with previous works (e.g., [Cornett, 2008]).

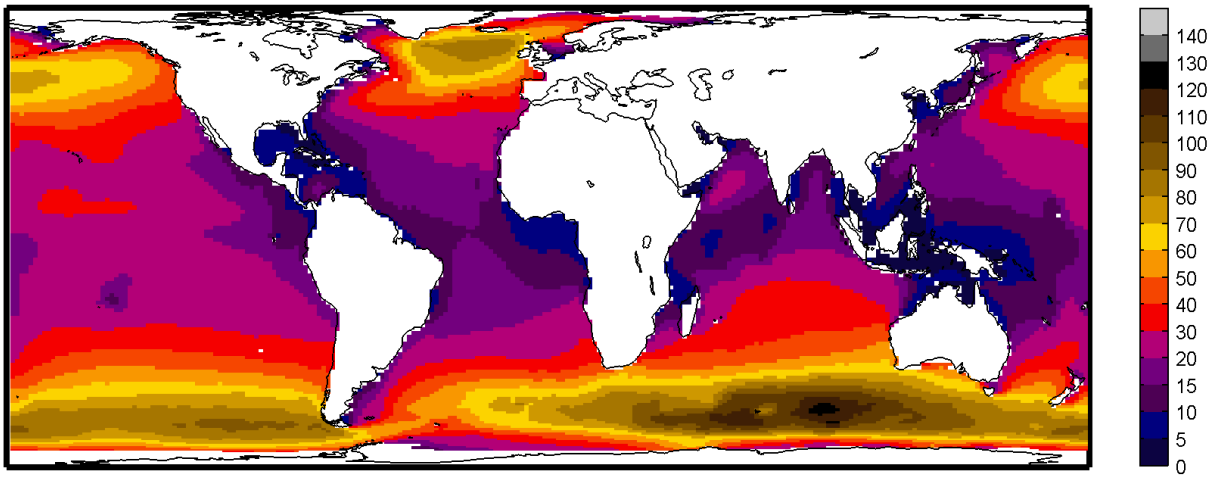

Figure 4.5: Mean annual wave power (kw/m). Computed from 1948-2008.

Since wave power resources are expressed in terms of kw/m of wave front (Figure 4.5) they correspond to the mean energy flux that crosses a cylinder of 1 m of diameter and the water column height. However, the theoretical resources along a certain coastline for exploitation purposes must be obtained considering the physical configuration and the actual length of the exploitation front (i.e. generally the coastline). Although the wave power patterns mostly coincide within works, the definition of the global theoretical wave energy vary depending on the different approaches and methods. This is why, since the early works in the last half of the last century ([Mollison et al., 1976, Isaacs and Seymour, 1973]), a considerable controversy around global wave energy estimation still exists.

The global offshore wave power was originally estimated to be between 1 to 10 Twh ([Isaacs and Seymour, 1973, IEA, 2009]). This figure is also usually presented in terms of the annual total power, expressed in Twh/yr. According to the World Energy Council ([WEC, 2010]), the global wave energy in deep water ranges on the former interval, with economically exploitable resources varying to a maximum of 2,000 Twh/yr ([CRES, 2003, Thorpe, 1999]), which is in the same order of magnitude as world electrical energy consumption. The IPCC Special

Report on Renewables Energy Sources ([Lewis et al., 2011]) includes [Mork et al., 2010] results providing a global estimate of about 32,000 Twh/yr and, for the first time, distribution over different regions of the world, including a theoretical potential a 8% lower due to unusable low wave power levels. This report also insists on the need of evaluating the technical potential of wave energy. The Greenpeace report on energy resources ([Teske, 2010]) estimates an overall available ocean energy of about 90,000Twh/yr, from which it is said that an important fraction corresponds to wave energy potential.

Considering this ample range of values, here a different approach for wave energy potential assessment is presented, resulting in an estimate considerably below current figures, about a 60% lower in comparison with the most recent results. It may be more adequate for technical assessment and closer to real available resources because it considers wave energy direction restrictions in exploitability estimations. Besides, results are supported by a global database with much longer time series.

The approach presented here is based on the fact that, every sea-state, represented by an energy flux vector, can cross orthogonally only a certain length, depending on the wave energy direction and coastline configuration (see Figure 4.6-b). This length will be referred to as *effective length* in the following as it represents the orthogonal length to the wave energy flux. This method considers that energy can not be harvested in all the extension of the coastline front, independently of the energy direction (see sketch in Figure 4.6-a), and keep important similarities with the approach by [Mollison, 1986] for western Europe.

In this work, to obtain a global assessment and regional resources distribution, the world coastline is discretized into a number of sections separated between 1 and 1.5 degrees from each other. The resource is hence computed at a total of 903 coastal sections, bounding each ocean basin, limited to deep waters off the coastline and considering the coast direction to define the effective coastal length. The coastline is finally divided into several sub-regions for the regional analysis of theoretical resources. The world coastline is classified into the following regions, represented in Figure 4.7: North and South America, western and eastern coasts, and sub-divided into north and south sub-regions by the Equator; hawaiian islands; Greenland and Iceland; European Atlantic coast; Africa, distinguishing western and eastern coasts; Madagascar; Australia and New Zealand; and Asia, divided into south, east and the polynesian area.

The wave power was computed hourly from 1948 to 2008 and the total energy for each year was determined according to the approach explained before (on a hourly basis). Following [Mork et al., 2010], the following criteria are considered: (i) the gross theoretical resource is calculated considering all contributions (hourly and yearly aggregated), (ii) unusable low levels of wave power (hourly values below 5kw/m) were not considered and (iii) the net resource, is computed after removing unusable low levels of wave power and points with ice coverage (ice coverage was identified at points located over 55°N and with more than a 5% of data missing).

Table 4.1 presents the results of the gross theoretical wave energy resources accounting for the energy flux direction. In addition to the mean values for the gross and net values, the standard deviation of the yearly mean values is also provided as a quantification of the range of variation within years.

The global gross theoretical wave power is approximately 16,000 Twh/yr (corresponding

to 1.8 Twh power). Its standard deviation is over 1.000 Twh/yr and the mean rate of long-term change is about 58 Twh/yr, which implies a sustained mean change of around 3,500 Twh during the last six decades (over a 20% of estimated mean theoretical wave power), that may be attributable to natural variability or climate change. On a regional basis, it is also detected that the western borders of the continents present greater potential and higher variability (represented by the standard deviation).

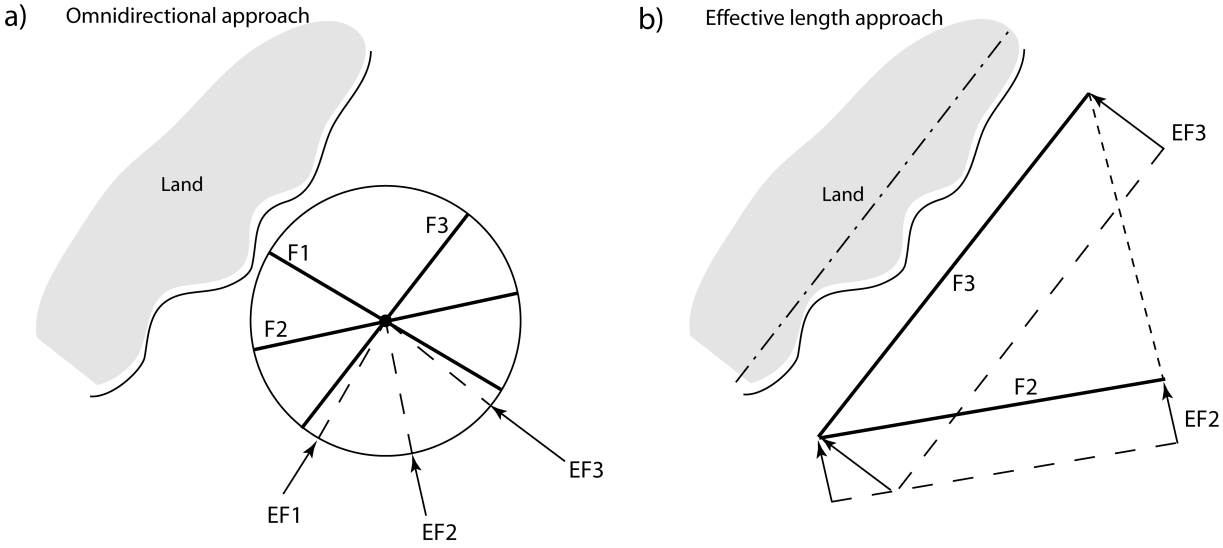

Figure 4.6: Sketch of the omnidirectional analysis of the energy flux vectors (a) and effective length of wave energy flux (b).

The regional assessment was also computed without considering direction of the wave energy (Table 4.2). The global gross theoretical wave power is over 3.3 Twh in such a case. This corresponds to a mean overestimation of an 83% if energy direction and the effective coast length are not considered. When excluding the unusable low levels (WP<5 kw/m) and points with presence of ice the theoretical resource decreases to 2.9 Twh. These values are very close to results reached by [Mork et al., 2010] with 3.7 and 2.9 Twh for global gross and net resources, respectively.

Some discrepancies with [Mork et al., 2010] can be explained. In the first place, [Mork et al., 2010] considered the Caribbean, the Mediterranean (evaluated in 171 Gwh for Central America, although they included the corresponding resources of the Pacific shore; and 37 Gwh of net potential for Mediterranean sea) and other interior seas that are not included in the study. Secondly, values are computed in this study on a hourly basis and, also, the length of the series used are longer, adequate for mean values estimation and showing a fine agreement with observations in terms of correlations statistics (see Chapter 2). A major difference can also be attributed to the different segmentation of the world coastline. Despite these drawbacks, the comparison of results is reasonable in some macro regions of the world such as: Australia and New Zealand, Africa and America.

In Australia and New Zealand, [Mork et al., 2010] estimated the resources to be 590 and

	Wave power resources (Twh/yr)					
REGION	WPgross	σ	Trend	WP	WPnet	σ
North America (W)	2,320.6	277.9	11.2	2,280.2	2,280.2	286.5
North America (E)	638.4	48.1	1.5	580.6	560.0	50.1
South America (W)	1,532.7	237.7	5.8	1,526.0	1,526.0	240.2
South America (E)	749.6	64.8	2.5	704.5	704.5	70.7
Hawaii	134.8	14.3	0.3	133.5	133.5	14.5
Greenland and Iceland	1,190.7	126.2	3.2	1,181.0	981.8	126.7
Europe (W&N)	1,573.0	175.3	5.7	1,546.3	1,530.3	176.8
Africa (W)	1,155.0	127,6	3,8	1,102.5	1,102,5	135.4
Africa (E)	644.6	50.3	1.7	602.9	602.9	53.0
Madagascar	363.6	33.6	1.1	354.5	354.5	34.7
Asia (S)	736,6	67,3	1,9	669,9	669,9	68,6
Polynesia	1,049.6	107.5	3.6	974,6	974,6	111,9
Asia (E)	1,091.3	135.7	3.2	1,041.2	1,041.2	138,1
Australia and New Zealand	2,844.6	286.0	12.5	2,808.1	2,808.1	287.6
GLOBAL	16,025.1	1,177.9	58.0	15,505,8	15,270,0	1,212.5

Table 4.1: Global and regional theoretical wave power resources (in Twh/yr). Left columns corresponds to the gross resource (WPgross), its standard deviation and the rate of change over the last six decades; the middle part (WP) excludes unusable low levels of wave power (discarding hourly values below 5kw/m); and the right part presents the net power (WPnet), which excludes low levels and temporally ice covered areas, and its corresponding standard deviation.

	Wave Power according to the omnidirectional approach (Gwh)			
REGION	WPgros	WP	WPnet	Mean ratio
North America (W)	459.7	452.9	452.9	0.63
North America (E)	133.4	122.7	117.7	0.59
South America (W)	288.5	287.4	287.4	0.66
South America (E)	176.7	167.7	167.7	0.57
Hawaii	51.7	51.4	51.4	0.32
Greenland and Iceland	297.2	294.7	238.0	0.48
Europe (W&N)	391.6	384.7	381.7	0.51
Africa (W)	197.2	188.6	188.6	0.62
Africa (E)	120.8	113.4	113.4	0.57
Madagascar	73,2	70.2	70.2	0.53
Asia (S)	125.9	113.4	113.4	0.60
Polynesia	182.4	164.4	164.4	0.58
Asia (E)	274.2	265.1	265.1	0.50
Australia and New Zealand	567.4	555.2	555.2	0.50
GLOBAL	3,339.9	3,231.7	3.167.1	0.55

Table 4.2: Global and regional theoretical wave power resources according to omnidirectional criteria (expressed in Gwh). Left column corresponds to the gross resource (WPgross), the middle one excludes unusable low levels of wave power (discarding hourly values below 5 kw/m; WP) and the right part presents the net power (WPnet), which excludes low levels and temporally ice covered areas (5% of gaps).

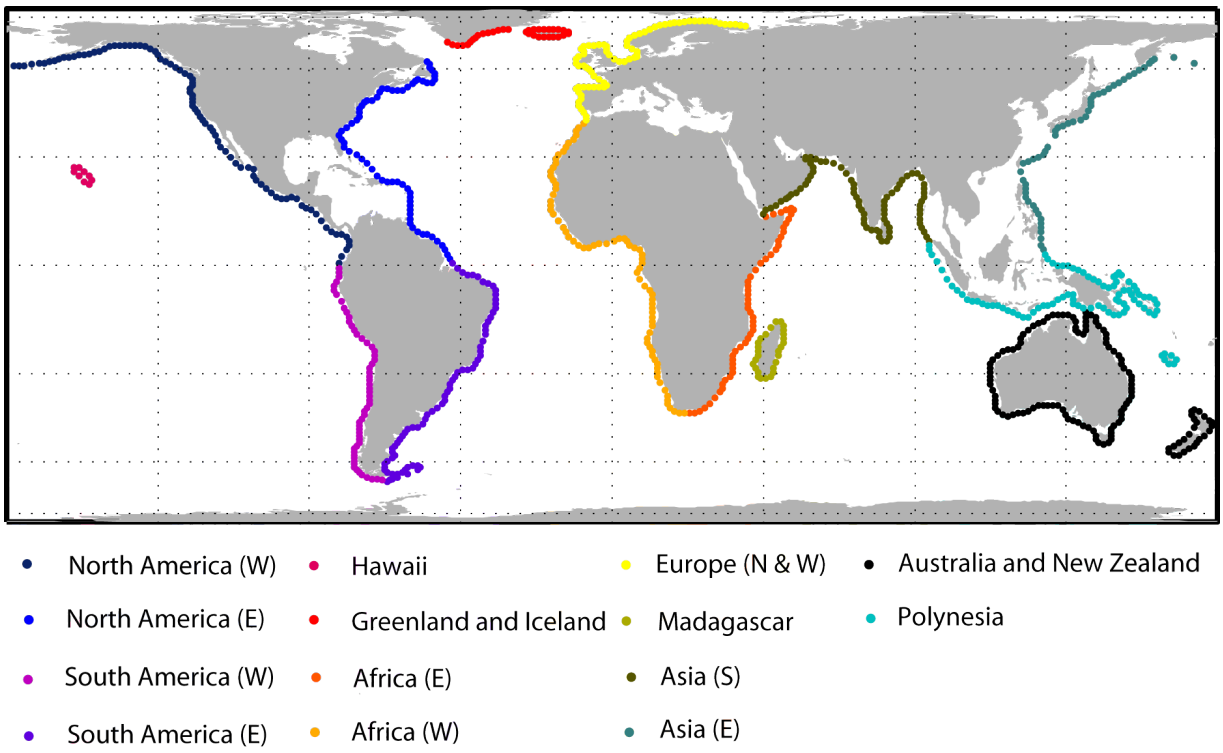

Figure 4.7: Coastline points and regions analyzed in the study.

574 Gwh for gross and net values respectively, which are very close to our 567.4 and 555 Gwh for the same area from our results (Table 4.2). The second area of comparison corresponds to Africa. [Mork et al., 2010] found a gross resource of 428 Gwh and net value about 422 Gwh. This analysis is comparable to our 391 and 372 Gwh (considering Madagascar). America is the largest area where a comparison is possible. Over such a big extension of coastline, [Mork et al., 2010] obtained 1,099 Gwh of gross resource versus the 1,058 Gwh obtained in this study, a small difference indeed. A higher deviation arises when considering the net resource due to the different ice coverage criterion; although the difference mean less than a 8%.

[Mork et al., 2010] found a reduction about 20% from global gross to net resources, the most important reduction due to ice coverage areas, especially important in northern Europe, Greenland northern America and the Russian coastline. In this work, the reduction is only about a 5% because the ice coverage identification is less restrictive.

The major difference between this work and previous assessments is due to considering the energy flux direction. Figure 4.8 displays the ratio between the theoretical wave power when considering the energy direction and the effective length. Tropical coastlines which are characterized by a strong swell component in the incident wave climate ([Young, 1999, Alves, 2006, Semedo et al., 2011b]) present values of this ratio over 80%. However, the northern Atlantic contour, the southern border of south-east America and several regions of the western Pacific coast (California is especially notorious) exhibit ratios about 50% which supports the need to take into consideration the present criterium for a more realistic assessment of deep water

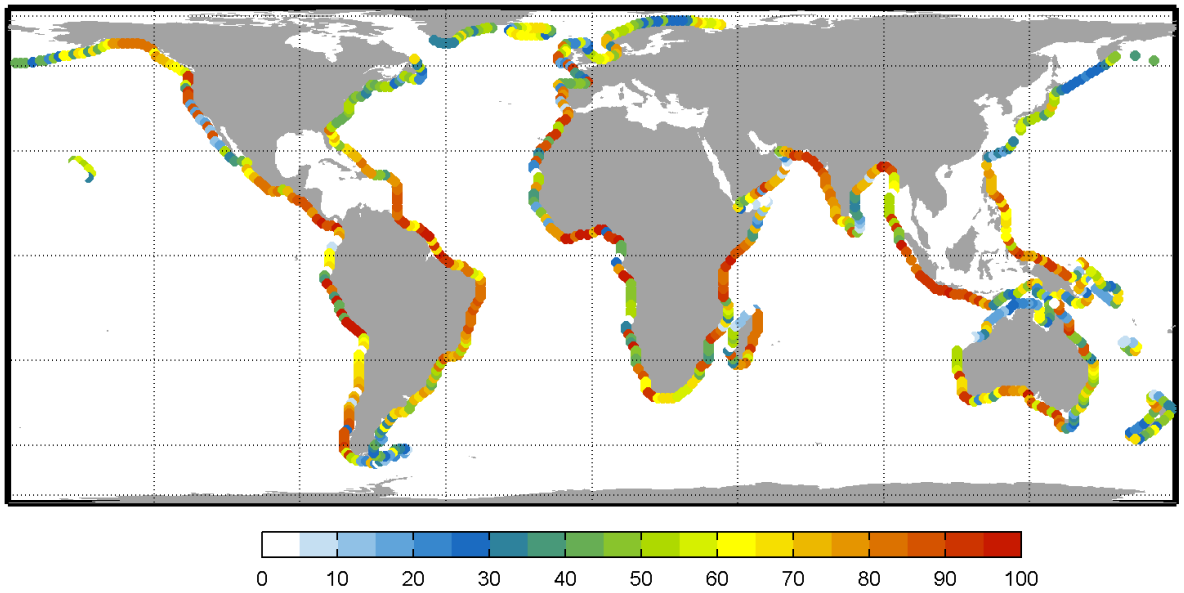

Figure 4.8: Ratio of variation of the gross resource considering the wave energy direction in the assessment (expressed in percentage)

theoretical wave power assessment.

4.2.2.5 Technical available wave energy resources

In addition to previous assessment discrepancies, the last report from IPCC remarks the scarceness of assessments on the technical potential on the various ocean energy technologies and future developments. Considering this fact and that previously presented figures are unconstrained by technical or economic considerations, some observations are set out in this section.

Theoretical wave power must be considered just as an estimate of the potential for harvesting. Meanwhile, the actual technical potential will depend upon technical development and efficiency, being considerably below the previous estimation. However, some reductions of the theoretical potential are independent of the device technology.

One critical challenge for successful design of WECs is the design wave. A WEC must be optimized to local wave power levels but its installation (mechanical structure and anchorage) must withstand extreme wave events further more energetic than standard conditions. Figure 4.9 displays the ratio between the 100-year return period significant wave height and the mean annual wave height. This ratio, following [Cruz, 2008], roughly reflects the ratio between the design cost for a wave energy plant, higher design waves requiring larger civil infrastructure; and the income, associated with the the mean resource. Low values of the ratio identify more recommendable areas for exploitation from the point of view of technical difficulty and cost.

The extreme wave statistics has been calculated with a Global Extreme Value distribution

(see [Méndez et al., 2007, Menendez et al., 2008]) fitted to the 61 annual maxima. However, note that in areas affected by hurricanes or tropical cyclones this ratio may be underestimated. To identified those sensible areas, the areas where more than a 0.6% of outliers were identified in the database after comparing with satellite altimeter measurements (see [Reguero et al., 2012b] and [Mínguez et al., 2012] for more details).

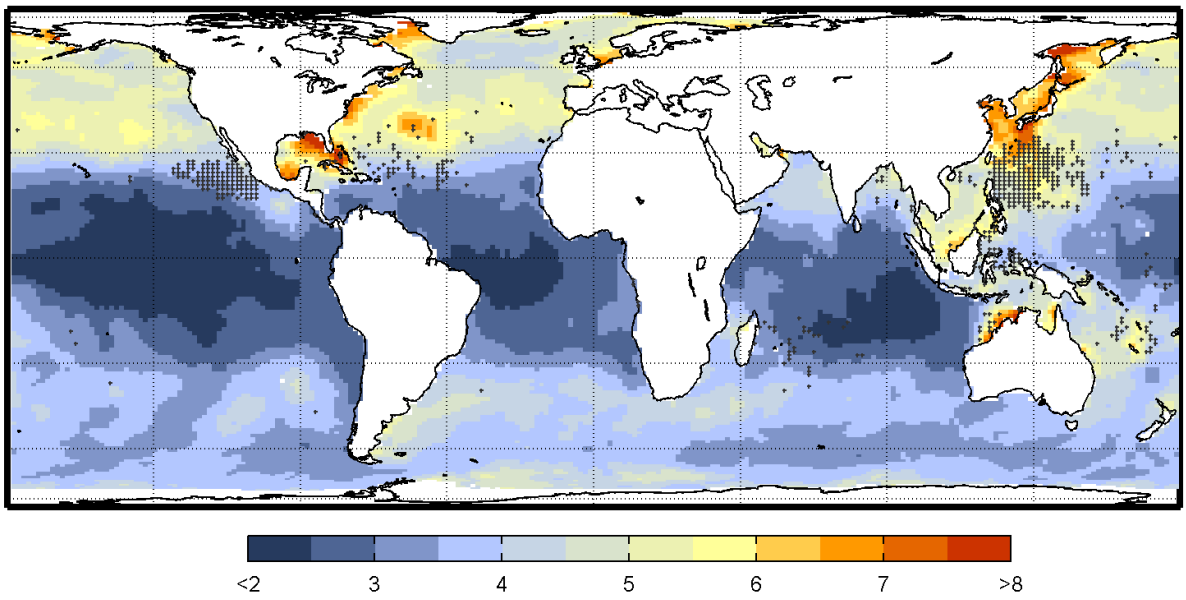

Figure 4.9: Ratio of the 100-year significant wave height to the mean wave height. The 100-year height is calculated with a Global Extreme Value distribution using the 61 year maxima in the dataset. The ratio is subjected to underestimation in areas affected by hurricanes and tropical cyclones, identified by markers in the graphic (areas with more than a 0.6% of outliers in the time series, compared with satellite data)

The most energetic sea states not only determine the design but they are also not exploitable. Therefore, the potential resources will be below the values expressed in the previous assessment. Even if this value is slightly dependent on technological issues and of each location, a typical value for the lost of exploitability under extreme events can be estimated to be about a 20%.

Another two challenges for design, waves random-nature induced, come from wave temporal variability in space and time. Wave power levels vary within months and seasons and depend on large-scale climate patterns as will be shown later in this work. Additionally, depending on wave directions, only a fraction of waves energy flux can be harvested, independently of the capacity of devices to rotate and point into the waves. These two factors are already included in the methodology since temporal variability is solved by computing the resources (hourly) for 61 years of analysis (in the period 1948-2008) being directionality of energy considered for the theoretical assessment.

One additional factor to decrease the theoretical resource independently of the device in concern is the different uses in conflict along the coastline. Protected areas, fishing areas or

maritime traffic lines are several examples of this lost of exploitable area. An orientative value for the reduction due to conflict of uses can be considered of about 0.8. For an adequate shallow water assessment similar methodologies to [Cruz, 2008, Camus et al., 2011] should be followed.

Considering these two factors (extreme events and conflict of uses) the mean theoretical global wave power resources previously calculated may be close to 10,000 Twh/yr. From this value, other reduction factors depending on each technology will reduce even more the usable resources.

In the case of the Spanish coast ([IDAE, 2010]) some efficiency factors were estimated for the Oscillating Water Column technology:

1. reduction for the absorbed energy from the total energy flux (hydrodynamic efficiency): 0.4

2. electro-mechanic losses in case of direct conversion (electro-mechanic efficiency): 0.8

3. efficiency and processing power electronics: 0.9

4. loss due to self consumption: 0.95

5. efficiency in transport and network connection: 0.9

An overall efficiency of about 25% from the theoretical resource can be estimated based on these technological restrictions, which means that only 2,500 Twh/yr will be available from ocean waves at offshore locations.

Refraction is the process that provokes most of the reduction in wave energy as the entire potential does not arrive at coast ([Folley and Whittaker, 2009]). A representative factor for nearshore resource is typically the 75% of the offshore power level ([Mollison, 1986]). However, a detailed study at each nearshore location is needed to define the spatial pattern of wave propagation and exact values of the resources potential. Several authors have already carried out nearshore wave energy assessments in the US Pacific Northwest ([Lenee-Bluhm et al., 2011]), California ([Wilson and Beyene, 2007]), Ireland ([ESBI, 2005]), United Kingdom ([ABP, 2008]), Portugal ([Pontes et al., 2005]) Canada ([Dunnett and JS., 2009]), the Baltic sea ([Henfridsson et al., 2007]) or Spain ([IDAE, 2010]).

The present assessment is only valid for offshore locations and as a consequence the list of available technologies is reduced accordingly. From the classification made by [Falcao, 2010] based on working principle, only floating technologies will be adequate for offshore locations.

Assuming a typical reduction for nearshore locations of 0.75 ([Mollison, 1986]), the theoretical available resources on world coasts will be of the order of 7,500 Twh/yr in average terms.

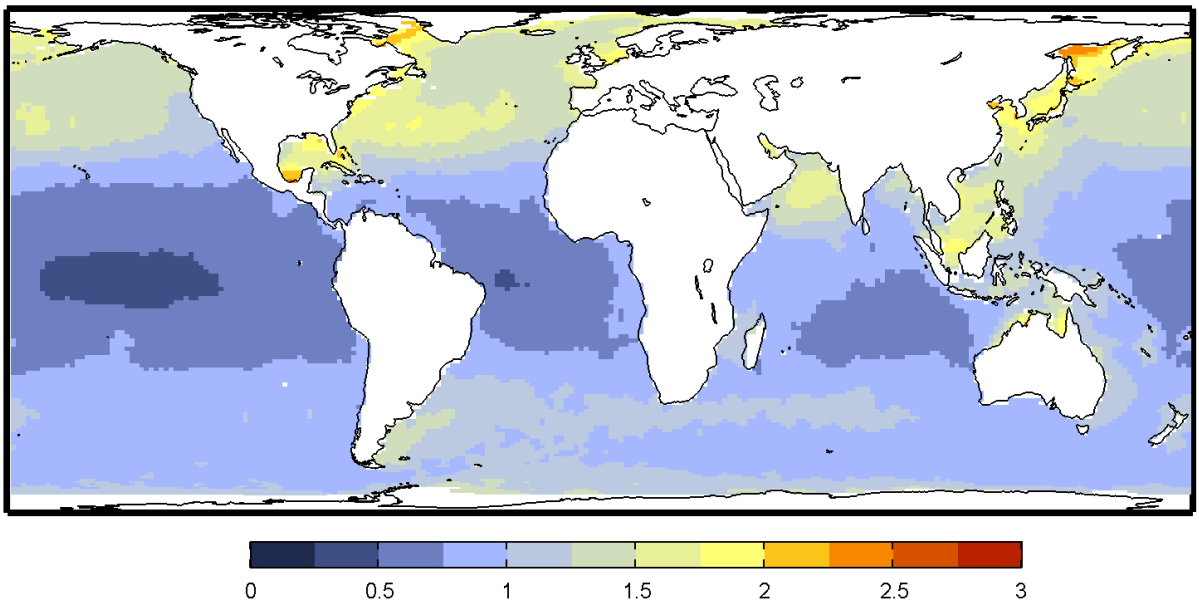

Figure 4.10: Coefficient of inter-annual variability of the energy resources from 1948 to 2008

4.2.3 Analysis of the temporal variability of the wave energy resources

4.2.3.1 Annual variability

The definition of the spatial distribution of mean wave energy is the first step for the resources exploitation analysis. However, the definition of the mean conditions is not sufficient and the temporal variability must also be studied to determine whether the changes throughout the year are important or not and, because WECs can be optimized for a certain range of periods and wave heights, decreasing efficiency with higher wave conditions variability ([Falcao, 2010]).

In an analogous manner to [Cornett, 2008], is studied here the temporal and spatial variability of the resource by means of some simple indices. To describe the temporal variability of wave energy, the coefficient of variation (COV), obtained from the standard deviation σ and the mean value μ is used:

$$COV = \frac{\sigma}{\mu} \tag{4.8}$$

The global spatial distribution of this coefficient is presented in Figure 4.10. These results keep great similarities with COV pattern obtained in [Cornett, 2008] by using a 10-year long time series, although some differences can be identified. For instance, in the Gulf of Mexico, the COV coefficient in Figure 4.10 exhibits values about 1.5 in most of the area. Similarly, a greater variability is detected in the NH, with values about 1.5 in the North Atlantic, while in the SH the index is generally lower than 1. The variability is distributed in latitude bands, although

some outstanding exceptions can be found in the Arabian Sea (values about 1.5), due to the wave generation of the Monsoon during June and July, and semi-enclosed basins such as the Gulf of Mexico and the Java Sea, with COV values of 2 and more.

Concerning seasonality, the mean resources have been studied in the four seasons, with seasons being defined as three month periods: December to February (DJF), March to May (MAM), June to August (JJA) and September to November (SON). Figure 4.11 shows the mean wave power seasonality, showing a winter peak in the NH (DJF) with values over 140 kw/m, and a strong decay during summer (JJA) with values around 30 kw/m. Likewise, in the SH the maximum values also exceed 140 kw/m, but in this case during the austral winter (JJA). Note that the mean conditions in the SH during the austral summer (DJF), with values over 60 kw/m, are higher than in the NH for the summer season. From Figure 4.11, a clear variability within hemispheres can be identified.

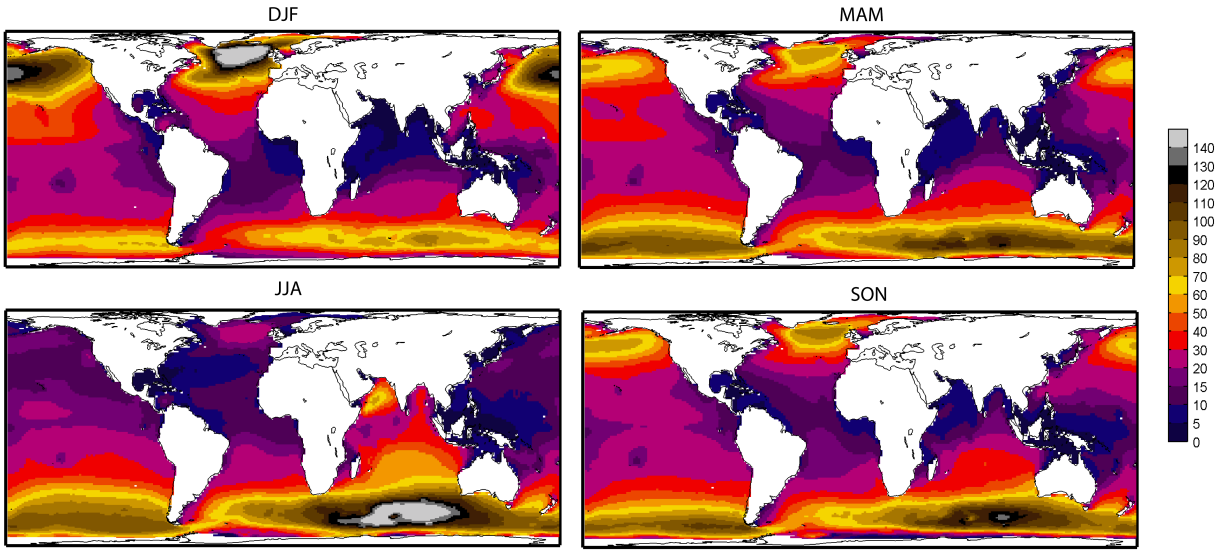

Figure 4.11: Mean seasonal wave power (kw/m)

In view of these results, conclusions reached in [Cruz, 2008] are confirmed for stable exploitable areas close to the coasts of: Chile, north-west of Mexico, west tropical coast and south border of Africa, west and south-east of Australia and most of the South Pacific islands nations.

Seasonality and monthly variations are studied by using seasonal and monthly variability indices (i.e. ratios of variation within maximum and minimum in seasons and months against the mean wave power) following the study in [Cornett, 2008]. Similar results were found, highlighting areas with marked seasonal behavior in the Arabian and Java Sea. Larger variability emerges again by this approach in the NH in comparison with the SH.

In the present study, to analyze the mean intra-annual varibility, the ratio of the minimum monthly wave power against the annual mean is depicted in Figure 4.12. Results are very similar for those obtained by [Cruz, 2008] for the same ratio. Figure 4.13 presents the same information showing the variation at each ocean basin against latitude. The red solid line indicates the latitudinal mean wave power for the corresponding basin. Both Figures further demonstrate the

great difference between hemispheres, with SH showing more stable conditions along the year. The range of longitudinal variation is also larger in the NH (see Figure 4.13). The spatial pattern keep great similarities with results in [Cruz, 2008] showing clearly that the lowest variability is to be found at the tropical regions, south of Africa and the south-west Pacific. A center of large variability is found in the southern Indian Ocean, explained by the presence of the Indian Ocean Anticyclone and its displacement westernward during winter, provoking a large seasonal change (see aforementioned works for more detailed explanations).

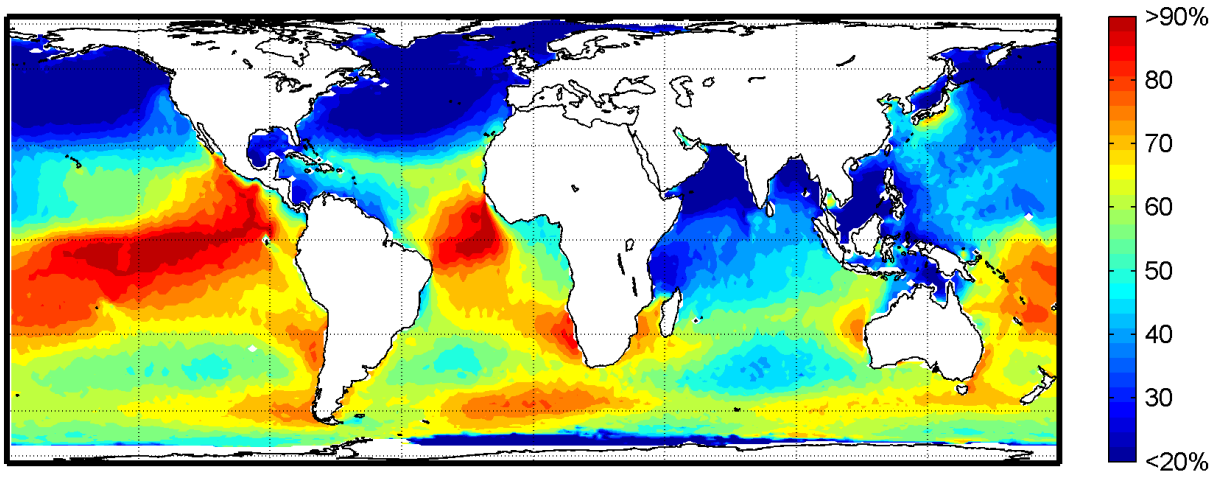

Figure 4.12: Ratio of the minimum monthly wave power to the mean annual value (expressed in %).

In view of these results, it is clear that the latitudinal temporal behavior is different at each ocean and hemisphere. Figure 4.14 represents the latitudinal variation of the mean wave power for each month along latitude (ordinates) at the longitude transects previously defined in the Pacific, Atlantic and Indian Ocean, but this time including the temporal variability along the year (abscissas). While in the NH the maximum values are reached at winter months, in the SH the maximum wave power is obtained at the summer season (austral winter). It is remarkable the large latitudinal variability in the three oceans and, regarding time, the large modulation of the resources in the North-Atlantic and South-Indian Ocean.

The previous representation provides a clear explanation of the average monthly variation. However, for each month, there exists a marked variation within years. The time span covered by the dataset allows a statistical descriptive analysis of the temporal variation on a monthly basis. Figure 4.15 illustrates the different temporal behavior of the wave power throughout the year for different points in the North Atlantic, North Pacific, North Indian and South Atlantic (coordinates are detailed in the figure). These plots introduce into the analysis a new perspective of variability as they show the mean and the 25^{th} and 75^{th} percentiles (black solid lines) of the averages for each month during the 61 years of analysis. Note that this representation evaluates the statistical distribution at each month of the year and, at the same time, it stands out the temporal variability within the year.

WECs are designed for a certain range of wave power values ([Falcao, 2010, Cornett, 2008])

and for exploitation purposes it is not only the mean but also the temporal variability within months and seasons of the wave energy necessary (i.e. represented by the size of each box in the box-plots). Higher variability in a certain month implies that the probability to expect values around the mean is considerably lower. In the North Atlantic and North Pacific, the temporal variability along the year reaches values over 100 kw/m in winter months and decreases to less than 50 kw/m in the summer time (corresponding with MV values between 1 and 2 and COV values about 1.5) with far less variation around the mean. Although the point in the North Indian Ocean is located at the NH, it shows a strong rise in summer months, both in the mean terms and its variability. Note the high variability, represented by the range between the 25^{th} and 75^{th} percentiles (black solid lines), which is notably large at that particular part of the year. This also occurs in the North Atlantic and North Pacific during the summer, from June to August (corresponding to months 6, 7 and 8). There is also a strong increase occurring in the South Atlantic during summer reaching 40 kw/m while the rest of the year it remains below 10 kw/m. This variability corresponds to MV values over 3 and COV values below 2.

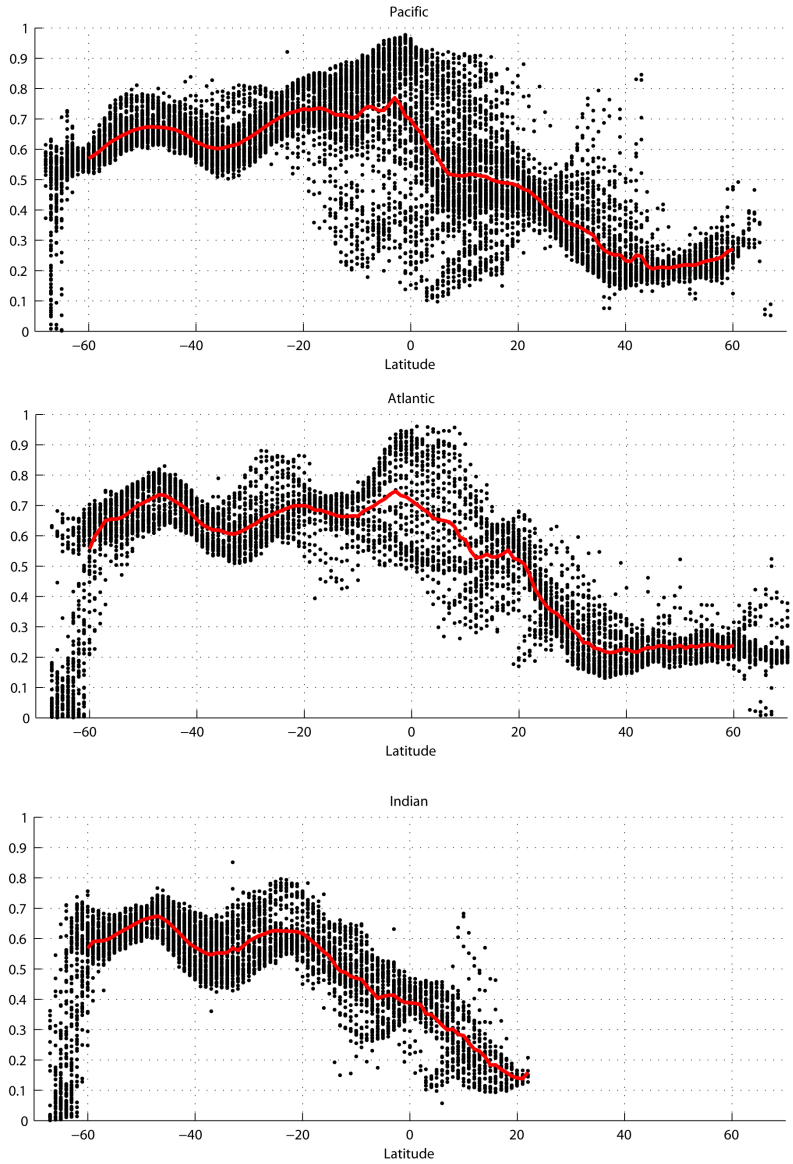

Figure 4.13: Latitudinal variation of the ratio of minimum mean monthly wave power to the mean annual estimate (from South to North) at each ocean basin. Basins are identified by the Pacific (upper panel), Atlantic (center) and Indian oceans (lower panel). Red solid line represents the mean value of wave power for each latitudinal band.

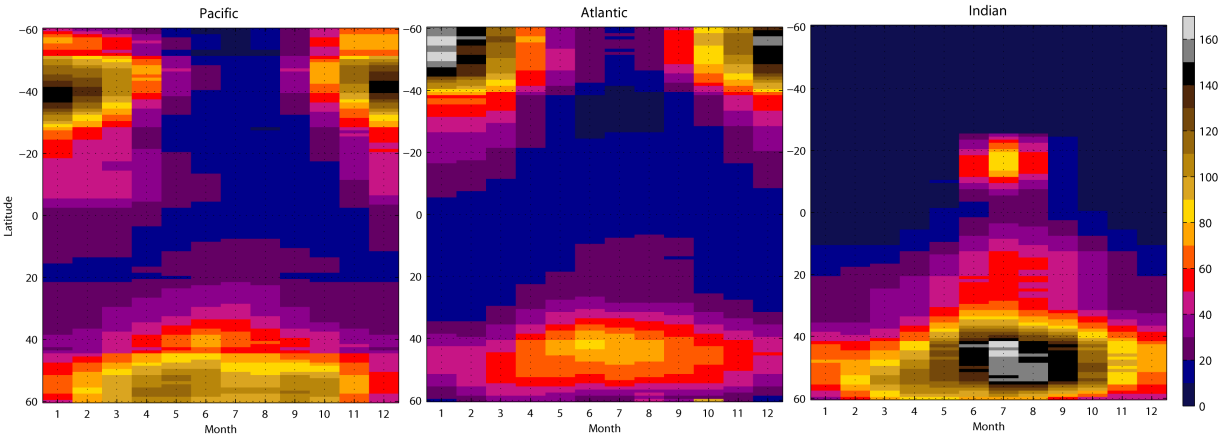

Figure 4.14: Monthly variation at the transects of mean annual wave power in the Pacific (left), Atlantic (center) and Indian Ocean (right). Months ranging from January (month 1) to December (month 12).

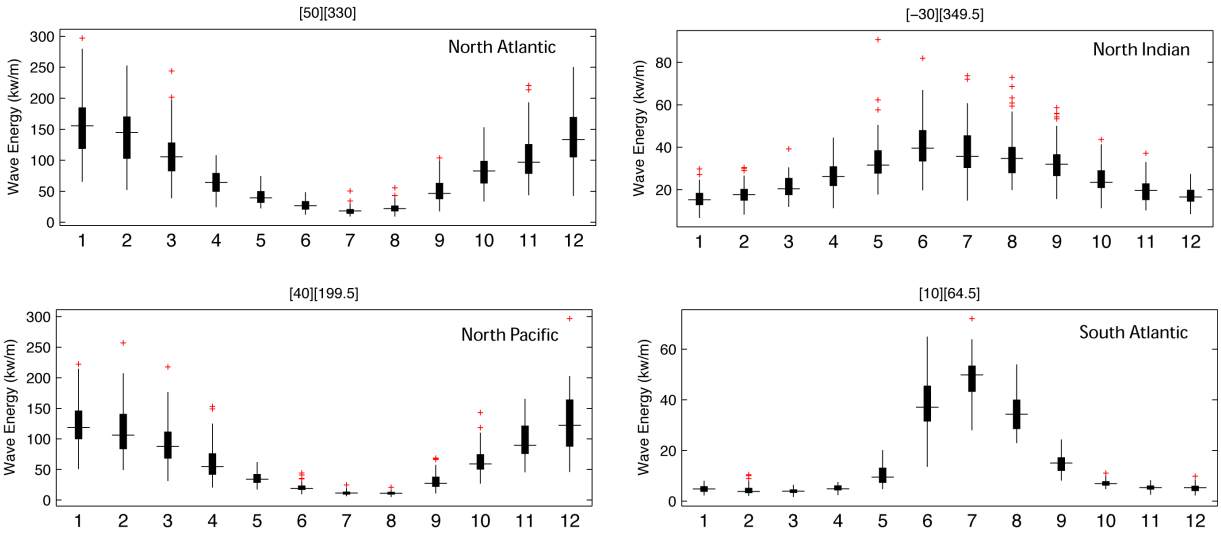

Figure 4.15: Temporal variability of mean wave energy within months for the period 1948-2008 for four locations (kw/m of wave front). Months ranging from January (month 1) to December (month 12).

Regarding the variability at each month, the range of values for the month with maximum mean value is significant at each location. During winter, the North Atlantic and North Pacific present values ranging from 75 to 275 and 50 to 210 kw/m, respectively, which corresponds to factors of variability in January between 3 and 4. On the contrary, in the Southern Indian and South Atlantic, maximum values are reached during summer. For the months with maximum wave power variability factors range from 2 to 3, or in terms of wave power, from 20 to 65 and 30 to 60 kw/m, respectively.

The variability of individual monthly means in the year is also large; power levels with a factor of 3 can be distinguished between the lowest and highest winter power levels in the North Atlantic and North Pacific, a factor of 2 between summer and winter in North Indian Ocean and reaching even a factor of 10 in the South Atlantic from the maximum to the minimum mean value.

Regarding the strong temporal variation of mean wave power resources (on a monthly basis) identified in these results, it is clear that planning, design and maintenance of exploitable wave-farms must consider this natural variability.

4.2.3.2 Resources inter-annual variability

Correlation analysis provides an identification of those areas where wave power resources are influenced by large-scale climate patterns characteristics of inter-annual variability. However, this analysis does not provide a measure of the influence magnitude in terms of wave power (in kw/m). To better understand the contribution of each pattern to wave power, the analysis must be addressed by incorporating the standard deviation (on a month scale) that has been removed previously. Based on the proposed regression model, the variation in wave power (ΔP) with respect to the climate indices values can be obtained as:

$$\Delta P_m = \beta \cdot \sigma_m \cdot \Delta CI^* \tag{4.9}$$

where ΔCI^* accounts for the change in the standardized climate index anomaly and $\beta \cdot \sigma_m$ represents the contribution to wave power per unit of standardized anomaly of the climate index for a particular month m.

Figure 4.16 includes a set of plots representing the spatial patterns of the Pearson´s correlation coefficient (ranging from -1 to 1, where 0 is null correlation and ± 1 means total correlation) between the wave power and several indices identifying which climate patterns are most influencing at each region.

In the Atlantic, the North Atlantic Oscillation (NAO), Scandinavian index (SCA) and the East Atlantic Pattern (EA) present a strong influence in the Atlantic wave power. The NAO pattern consists of a North-South oscillation of the pressure fields. When the NAO index is high, the westerlies are stronger than average which implies an increase of wave power over 40°N in the Atlantic and a sink around 35°N. The influence of NAO index in the northeast Atlantic can be associated to swell variations ([Gulev and Grigorieva, 2006]). As one can see in Figure 4.16,

the NAO index has a significant influence in the North of Europe showing positive correlations of 0.5 over the 45 °N in the North Atlantic. This result agrees with previous studies such as [Woolf and Challenor, 2002] who found correlations between 0.1 and 0.5 with the significant wave height in the area. Significant low correlations of 0.1, are found on the North Pacific, South Atlantic and Indian Ocean, which depicts smooth teleconnections between the North Atlantic and distant areas.

The Artic Oscilation (AO) and the Southern Hemisphere Annular Mode (SAM) are the patterns with wider influence in both hemispheres, respectively.

With respect to the SAM mode, a positive phase of the index is associated with a center of low pressure in the South Pole and a ring of high pressure anomalies at mid-latitudes. This leads to a zonal wind anomaly in a broad band around 55°S with stronger westerlies, that provokes an increase in wave power at southern latitudes, a negative correlation below 50°S from the Atlantic to the Indian, and small positive correlation along the South-East Pacific affecting the full coast of the Western America. SAM shows a widespread influence in the SH wave energy (consistent with [Hemer et al., 2010]) reaching positive correlations over 0.4 at high latitudes in the SH, which agrees with a strong wind speed intensification in the area. This pattern has a whole basin effect due to propagation of swells generated in the SH. Negative lower correlation is also obtained along a band at the southern border of Africa.

The results show that in terms of correlation with the wave power the influence of the AO is widespread in the NH with high positive correlation in the north Atlantic and strong negative correlation below 40°N and slightly lower in the northern Pacific Ocean. The positive phase of this index is related to lower pressures in the Arctic which results in a deviation of the storms to the North with an intensification of the westerlies. This leads to an intensification of the wave heights and periods in the North Atlantic over the 50°N with dominance of the West to north-west directions. Like NAO, this climatic pattern is also related with a strong decrease in wave energy in the Atlantic and moderate in the Pacific, both between the 25 and 40°N. This pattern is also correlated with a decrease in the Southwest Monsoon intensity.

The EA pattern ([Barnston and Livezey, 1987]) also consists of a North-South pressure dipole in the Atlantic, in this case spanning from East to West and with the anomaly center displaced southeastward. This pattern provokes a general increase in the East Atlantic reaching the tropical Atlantic with a maximum correlation around the 40°N associated with swells shifting to North-West direction, as previously stated by [Izaguirre et al., 2011] for wave heights.

Compared with the latter two patterns, the SCA index ([Barnston and Livezey, 1987]) shows weaker correlation and affects mainly the North of Europe because the anomaly center is located in the North of Siberia and the Arctic decreasing the wave generation in the area of the North Atlantic. This pattern presents another center of opposite sign in the West of Europe and over Mongolia that is associated with a weak increase in the wave power in the Atlantic and a dumping in the Yellow Sea.

The Tropical Northern Atlantic Index (TNA) is an indicator of the surface temperature in the eastern tropical North Atlantic Ocean and was defined by [Enfield and Mayer, 1997]. Positive correlations with wave power are found broadly in the Pacific and most of the Atlantic with the exception of negative influence in the southwest tropical Atlantic, northern Europe and south

Asia coasts.

Finally, the ENSO phenomenon identified in the SOI index shows a positive low correlation (r from -0.2 to -0.3) in the Pacific ocean, reaching positive 0.3 at South-America and extending its influence westernwards in the Pacific. A teleconnection in the southwest tropical Atlantic and mid Indian Ocean during negative phases is also detected.

One of the most prominent modes of low-frequency variability in the NH affecting the Pacific Ocean is the Pacific North American pattern (PNA). The PNA pattern is associated with strong fluctuations in the strength and location of the East Asian jet stream and with an eastward shift in the jet exit region towards western North-America. In terms of wave power, these winds affect positively in the north Pacific extending their effect until the 25°S, reaching the peruvian coast. Negative lower correlations, associated with a decrease in the wave power are found in the tropical southwest Atlantic and west Pacific.

The Western Pacific index (WP) was described by [Barnston and Livezey, 1987, Wallace and Gutzler, 1981] and consists of a north-south dipole of anomalies with one center over the Kamchatka Peninsula and another broad center of opposite sign located over southeastern Asia and the western south tropical Pacific. This climate pattern modifies the East Asian jet stream provoking a dampening of wave energy between the 25 and 50°N and an increase outside that latitude band, specially remarkable at the east of the said peninsula. Other teleconnections with negative phase of this index are found in the North tropical Atlantic and south Indian Ocean.

Another climate pattern affecting wave power in the Pacific is the East Pacific - North Pacific pattern (EP-NP) which presents three main anomaly centers, the positive phase featuring positive anomalies over Alaska and Western Canada, and negative anomalies over the central north Pacific and eastern north America. Positive phases are associated with a southward shift and intensification of the Pacific jet stream from eastern Asia to the eastern North Pacific which generates waves from East to West in the North Pacific and heavily decrease the wave power that reaches the whole western coast of America, from north to south. Weaker influences are found along scattered areas of the Atlantic and the Indian Ocean, generally close to coastal areas.

Finally, two climate indices representative of the Indian Ocean has been studied, the Indian Ocean Dipole (IOD; [Saji et al., 1999]), measured through the Dipole Mode Index (DMI), and the Quasi-Biennial Oscillation (QBO) also known as Singapore Winds (not shown). The correlation analysis with wave power shows a decrease in the resources in the mid Indian Ocean and at south America with positive phases of the index. Weak positive influence is found along several regions of the Pacific and the south Atlantic and Indian Oceans.

Considering the relationship of wave power with wave heights, most of the previous results agree with those from [Izaguirre et al., 2011] obtained for the extreme wave heights by using altimeter data.

Figure 4.17 explores the contribution to wave power (in kw/m) of some climate patterns. The correlation and the contribution to wave power in absolute magnitude describes how the wave power varies per unit of the standardized anomaly of each climate index but depends on the variability (i.e. standard deviation) of the wave power.

Therefore, the contribution of several climate indices for months December and June, chosen as representative of the summer and winter seasons at both hemispheres, was computed (not shown). It is also interesting to express the results in relative terms with respect to the mean resources value, as the same contribution in kw/m in two areas with different available mean wave power can explain very different proportions of the resources.

The PNA pattern shows a contribution of over 20 kw/m in the North Pacific during December in the NH, while in June the influence decreases to less than 4 kw/m due to a lower variability (i.e. standard deviation) during the summer, as previously seen in this work. When expressing the results relative to the mean wave power in June and December, these values explains about a 10% of the resources along the western border of America from north to the Equator at both months. In the North Pacific the influence counts for a higher percentage during the summer because the wave power is smaller.

The SOI pattern exhibits a stronger monthly modulation in the south Pacific and sustained weak contribution in the rest of the Pacific and Indian Ocean. During both months the contribution implies around 10% of the mean resources in the western border of South America and a reduction of the same magnitude in the north and west Pacific per unit of positive phase. It is remarkable that during December the percentage of resources explained by the latter two indices in the north Indian Ocean, along the Arabian Peninsula coast, implies a wide spread increment between 10 and 25% for the SOI positive phase, and a decrease for the PNA limited in space.

Concerning the Atlantic, AO and EA contributes with more than 20 kw/m in the North Atlantic in December. As seen in the correlation patterns, EA influence shifts an increase southward reaching the tropical Atlantic while AO increases wave power over the 50°N (well over 15% of explained mean wave power anomaly throughout the entire year) and decreases about 8 kw/m in the rest of the Atlantic and the northern Pacific, reflecting different directions of swell propagation for each index (EA southwards and AO easternwards). The values obtained in summer are much lower.

The SAM index explains a large fraction of mean wave power variability in the SH. In June the contribution to wave power is slightly higher than in December but this modulation is not so intense as seen for other indices, because the wave power, although large, is partially maintained along the year (i.e. low variability). Opposing to what happens in the NH, the influence of this climate pattern is more notorious (over 25% during December (austral summer) because the wave power is lower. However, the change is not so strong as seen in other cases because of the lower variability in the area.

EP-NP reflects a weak modulation of the wave power in the north Pacific affecting western North-America from Alaska to California. This case is interesting because a dipole is clearly identified in terms of wave power magnitude but in terms of correlation this pattern was not that clear (owing to the variability). In relative terms, the influence is larger in June with the exception of the north Indian Ocean (not shown).

The WP influence in the Pacific is remarkable as it explains more than a 10% of the resources variability along the western border of North America and eastern Asia. It shows a larger effect in summer but it is maintained during winter.

Several conclusions arise from the analysis of the variability of the resources. Firstly, although the effect of a climate index in the wave power is larger in magnitude when the resources are high (i.e. winter season); it is during the summer months, when the wave climate is milder, that the presence of a certain climate pattern affects more. Secondly, in the North Indian Ocean, a region with strong variability in the resources, the effect of climate patterns is significantly remarkable in winter, when the variability range is larger.

Finally, it can be confirmed that natural variability is a greater factor to consider in wave energy exploitability and design issues. Additionally, in some cases (like in the SH for the SAM) inter-annual variability has been shown to be in the order of magnitude of mean seasonality.

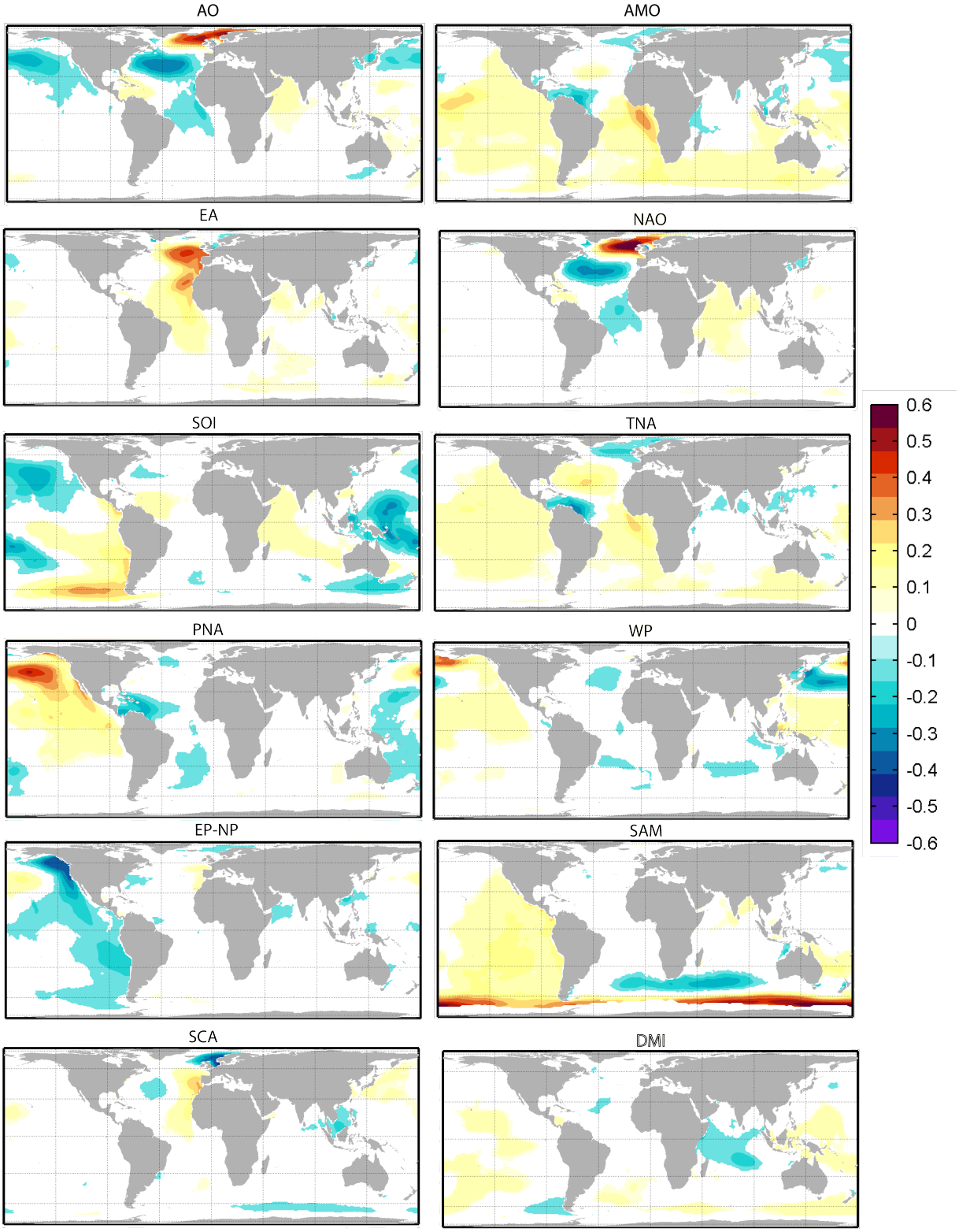

Figure 4.16: Linear correlation of wave energy resources with several climate indices.

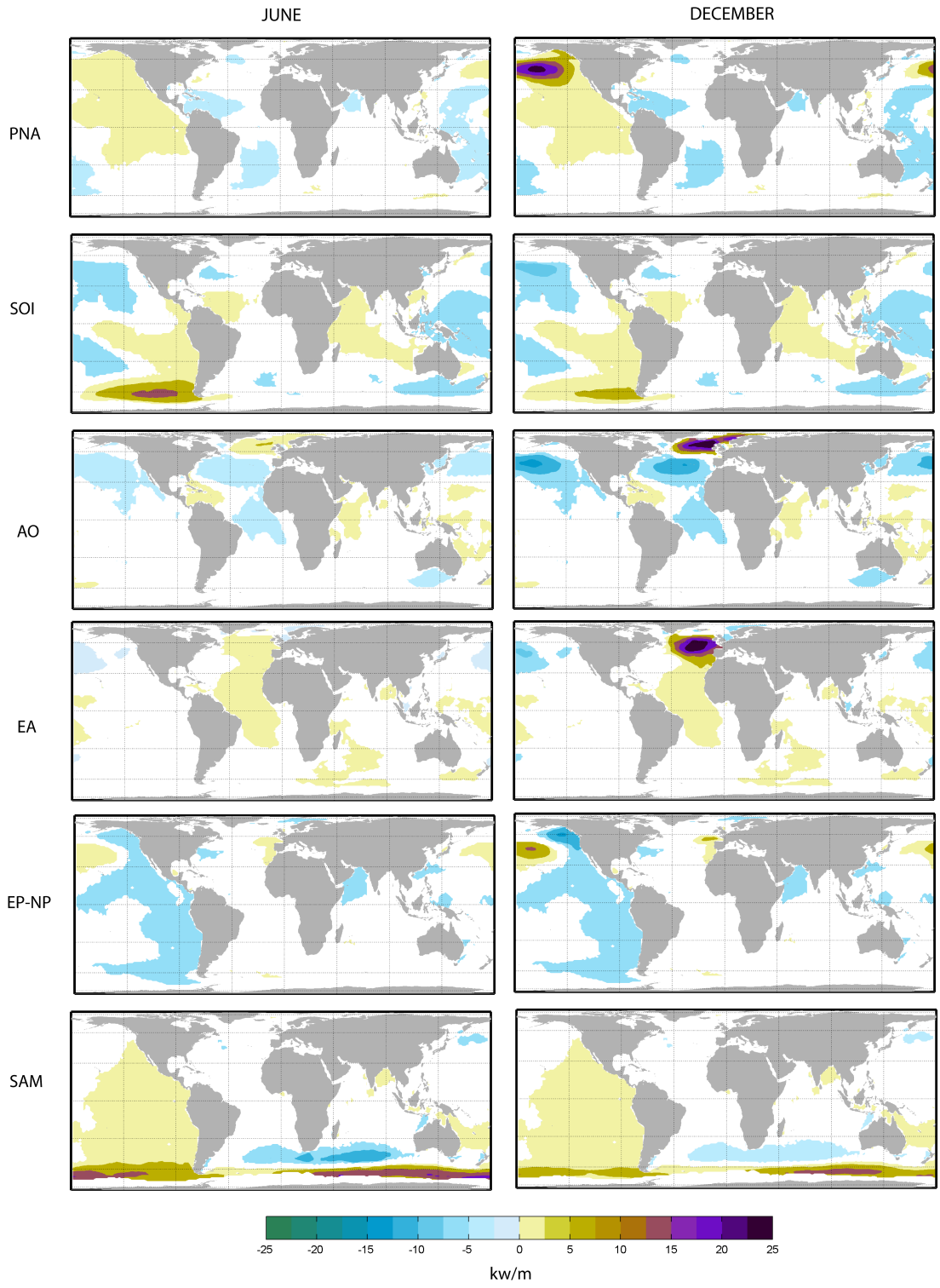

Figure 4.17: Mean contribution to wave power (kw/m) per unit of standardized climate index anomaly.

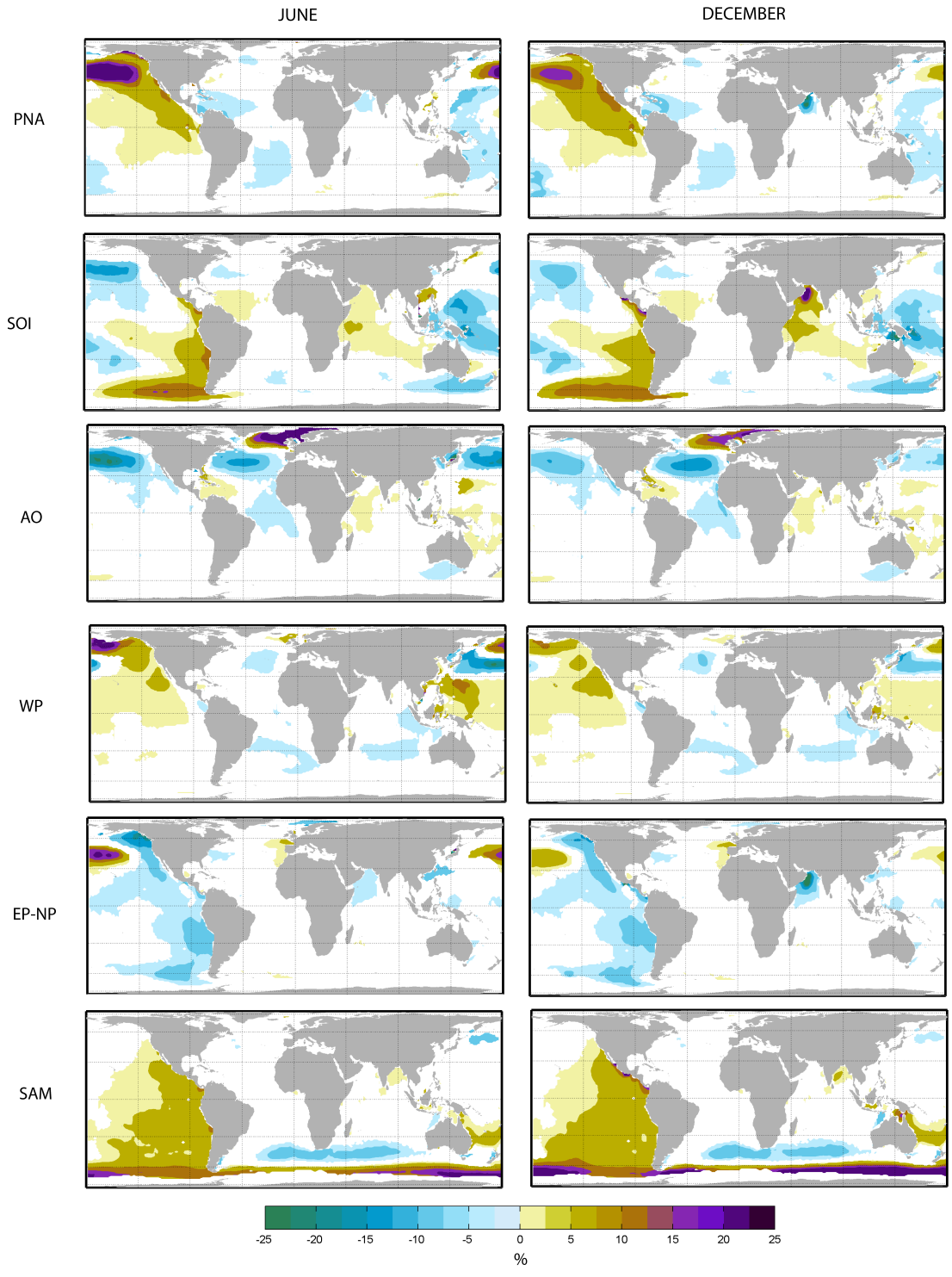

Figure 4.18: Mean contribution to wave power with respect to the mean value (%) per unit of standardized climate index anomaly.

4.2.3.3 Long-term trends changes

Many studies have analyzed measured or reanalyzed data to detect trends of change in past wave climatology. Studies based on wave hindcasts ([Group, 1998, Cox and Swail, 2001, Wang and Swail, 2002, Sterl and Caires, 2005, Hemer et al., 2010, Dodet et al., 2010]) based on NCEP/NCAR or ERA-40 reanalysis winds have shown a growing mean H_s as well as an intensification of H_s extremes during the last four decades of the last century. In the northeast Atlantic in particular, the 99th extreme of the winter H_s increased by a maximum of 40 cm per decade ([Wang and Swail, 2001, Caires and Sterl, 2005a]). In the northeast Pacific, buoy records report growing wave heights for the period 1978-1999 ([Allan and Komar, 2000, Gower, 2002]) with increasing values from 1.2 to 2.7 cm/yr, also reflected in the extremes ([Menendez et al., 2008]). The results to be presented here are also consistent with these findings.

In the present work, long-term changes are derived from the GOW dataset for the period 1948-2008. Considering the length of the simulation period, it is possible to study the long-term changes in the wave energy resources over the last six decades to determine if climate change is affecting the wave energy resource and quantify it. The trend was computed as a linear function over the duration of the time series and the statistical significance was checked using a Student´s t-test. Given the wave reanalysis spatial resolution, the trend is representative of a 1.5°x1.0° region.

The linear trend patterns in annual wave power over the period 1948-2008 are shown in Figure 4.19. The trends are obtained by linear least squares fits to the yearly time series of wave power (see Figure 4.20 where 1-hour wave power time series are plotted along with the average value every year and the regression linear fit). The most energetic regions in the global ocean, in the SH (see Figure 4.5), are increasing at the highest rates with trends from 0.4 to 0.8 kw/m/yr. North Atlantic and North Pacific are experiencing a moderate increase of 0.2 kw/m/yr. Results show that no significant trend is occurring in the North Atlantic below 45°N. These results are in agreement with previously detected trends in wave climate statistics (see previous sections) in the SH ([Hemer et al., 2010]) and NH (e.g. [Dodet et al., 2010]).

Linear regressions have also been performed for anomalies over each season. Figure 4.21 analyzes the trends studying each season separately. Again, a different behavior is identified between the NH and the SH. In the SH, the trends are relevant along the entire year, although of greater magnitude during the austral winter. On the contrary, during the summer, the North Atlantic trends are not significant and very weak in the North Pacific. However, during winter, the trends strengthen over 0.5 kw/m reflecting an increasing trend in the resources only at the stormy season.

The different trends detected within seasons in the NH have important implications for exploitation purposes because previous results indicate that the range of variability of wave power between mean monthly values is increasing with respect to summer resources availability. Furthermore, this is occurring in an area with already high variability range within the year, accordingly with results.

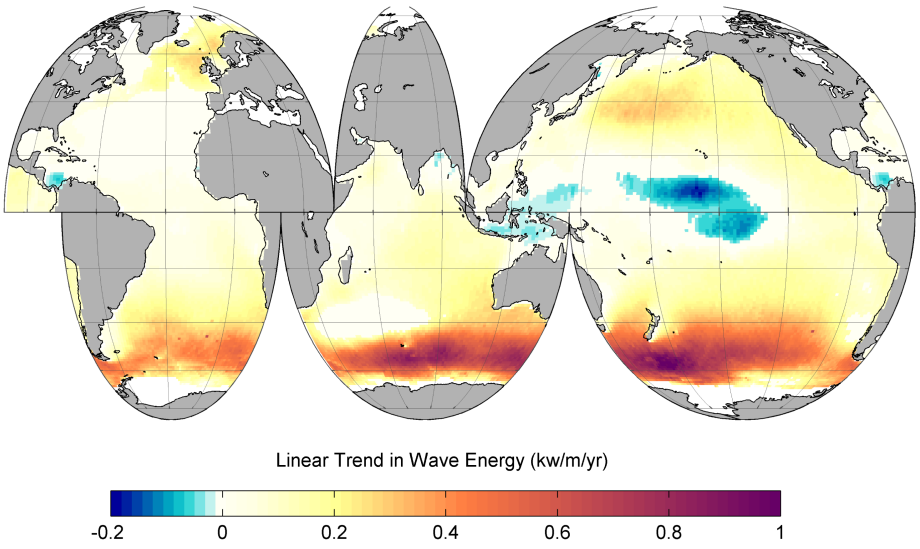

Figure 4.19: Annual long-term trend in mean wave energy resources from 1948 to 2008 (kw/m/yr).

Figure 4.20: Long-term changes in mean wave energy resources from 1948 to 2008 (kw/m) at two locations in the North-Atlantic (upper panel) and in the South-Pacific (lower panel). Hourly time series of wave power (gray), yearly mean value (black) and long-term trend (red) are represented.

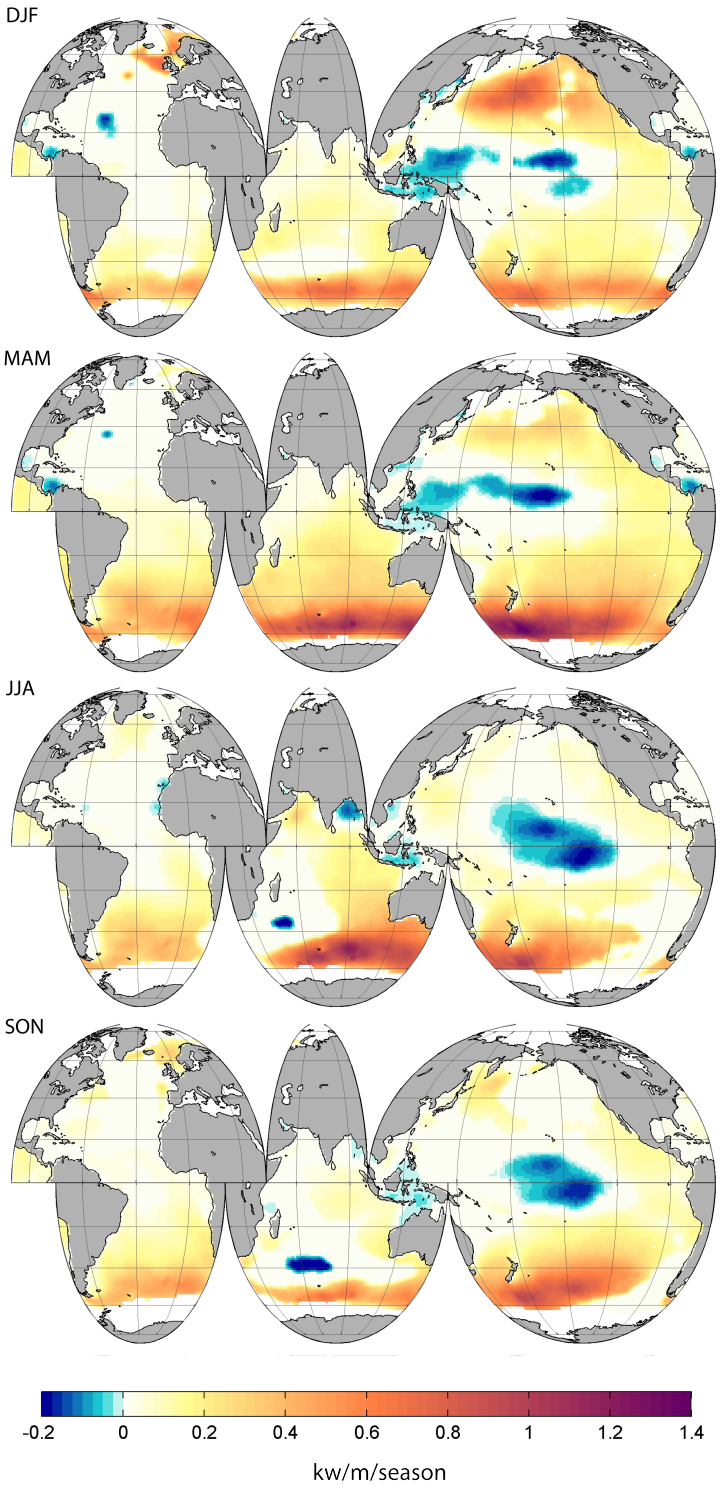

Figure 4.21: Seasonal long-term changes in mean wave energy resources, computed from 1948 to 2008 (kw/m/season).

4.2.4 Variability of wave energy along the continental margins

The variability of wave climate has become clear in Chapter 3 of this work, both in space and in time. However, this vision of the climatology relies on the description of certain statistics, like the mean annual significant wave height, for example, to study its spatial and temporal variability. To see the variability of the wave energy resources in terms of the wave climate parameters, a different vision is needed.

This time, the focus is set on the distribution of wave heights and periods. This is usually overcome with scatter diagrams of energy or frequency of occurrence for each pair of wave height and period (in this case, H_s and peak period, T_p). The theoretical wave power for each pair of H_s and T_p (Figure 4.22) can be easily obtained from equation **??**. From the hourly time series in the GOW database, the set of occurrences and the annual wave energy for each combination of heights and periods can be easily defined.

Figure 4.23 represents the histograms of annual wave energy for 10 points at deep water along the world coastline. The differences in shape and intensity of wave energy is evident for the points at high latitudes, in both hemispheres. This representation is indicating where the main energy, along the year, is concentrated. For example, for point 5 (North-Atlantic coast), the largest amount of energy along the year come from sea-states with periods around 12 s and 4 m. For design of wave farms this information is crucial as the WECs must be designed for the optimum wave period that maximizes production. In the SH the range of periods where the energy is concentrated is larger due to the widening of the storm area during seasons, but with a sustained intensity.

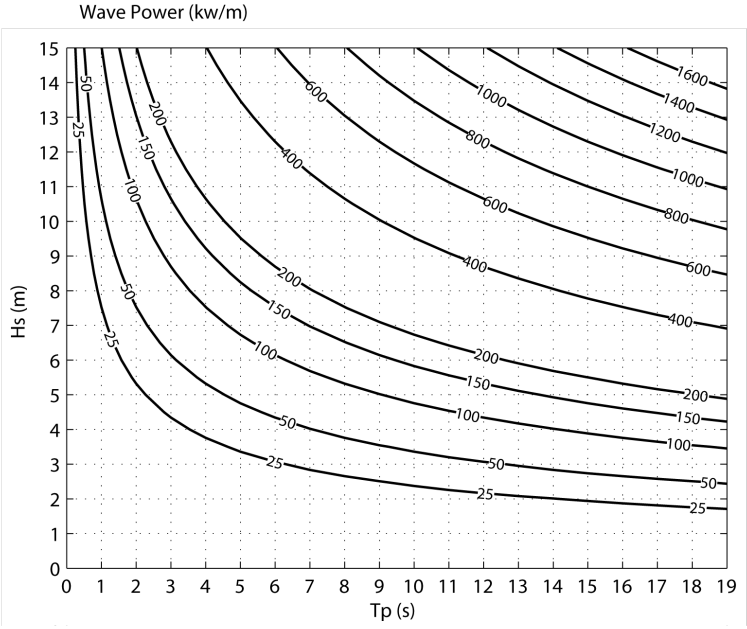

Figure 4.22: Contour plot of wave power (kw/m) for a certain range of peak period (Tp) and significant wave heights (Hs).

Instead of wave energy density, Figure 4.24 represents the set of occurrences for the same 10 representative points, shown in Figure 4.23. By crossing these histograms with the theoretical wave power (histogram in Figure 4.22, represented at each plot) the total wave power could be obtained for each point. A more intense color means higher frequency of each pair of height and period. The higher concentration of the distribution indicates a less variable wave climate.

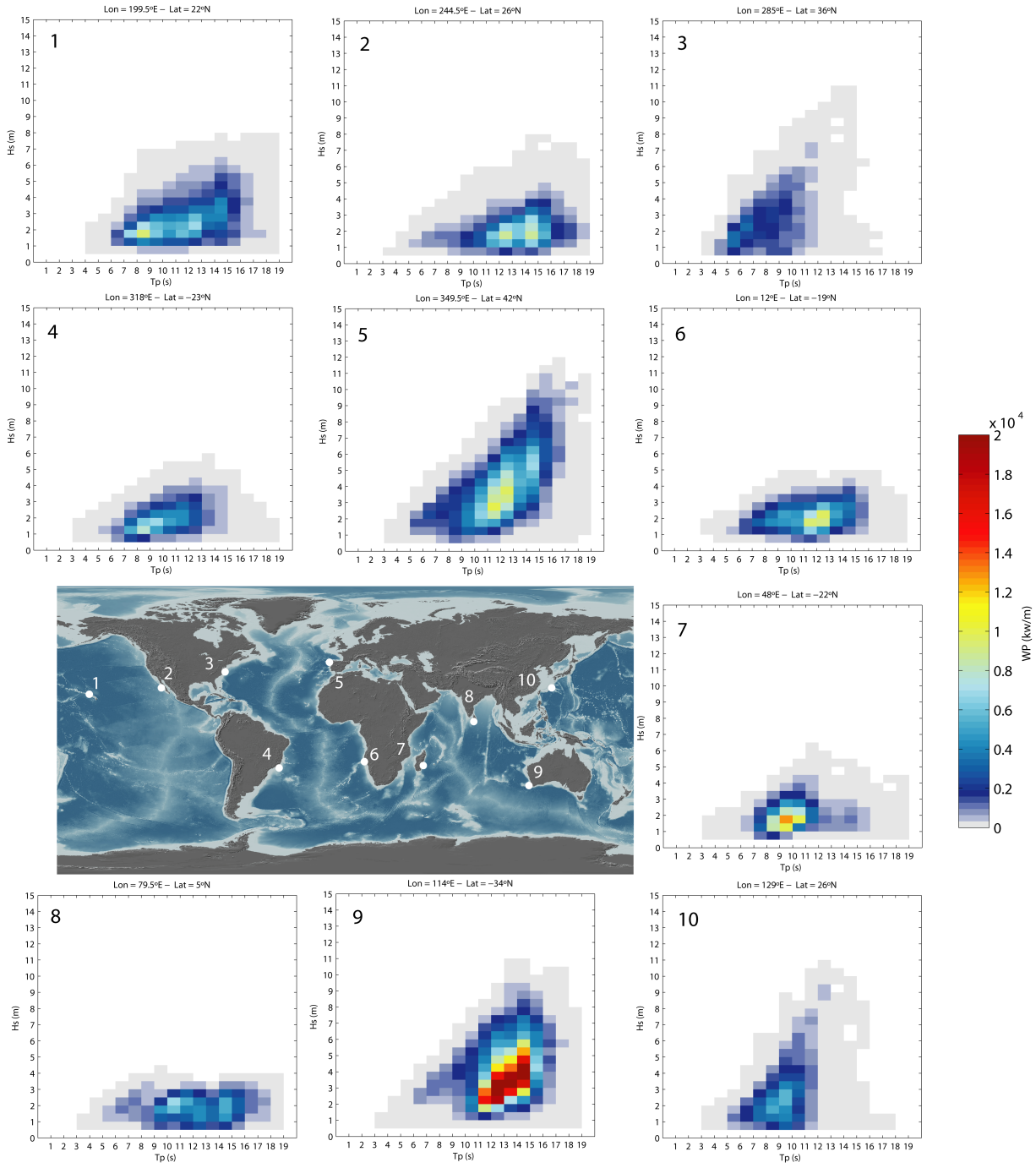

Figure 4.23: Histograms of occurrence and wave power scatter diagrams at ten representative points along the world coastline.

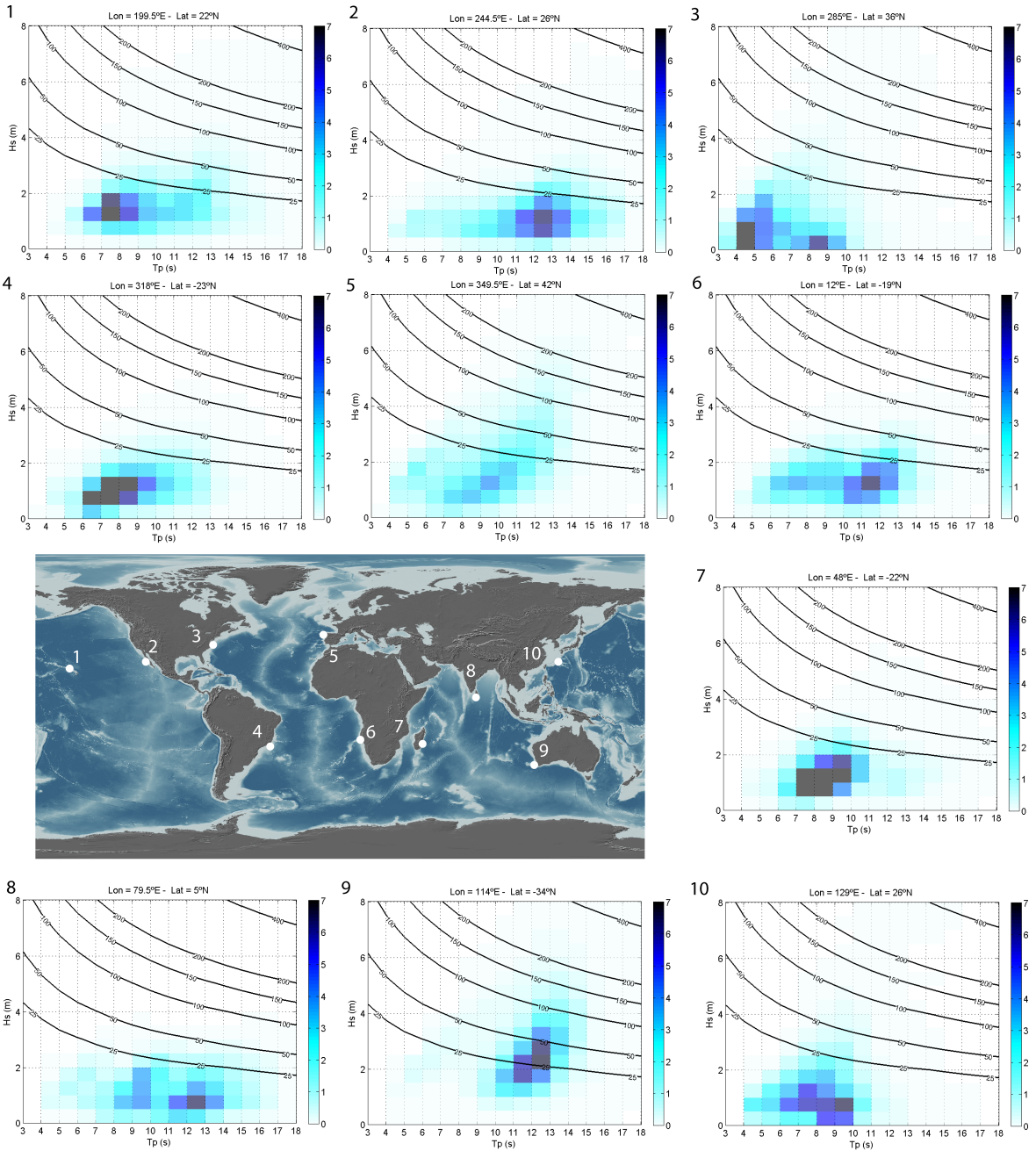

Figure 4.24: Wave power levels and scatter diagrams of frequency of occurrence (%) at representative points along world coastline.

4.3 Technological risk analysis

4.3.1 Introduction

In the last decade many projects for the development of wave energy converters (WECs) have emerged in places all around the world, especially in Europe. A review of technologies and working principles may be found in [Falcao, 2010].

The aim of this work is contributing to clarify what can be reasonably expected as the mean output of several technologies of WECs at offshore depths worldwide by proposing a method to consider the variability and long-term changes of available resources coupled with simplified optimal designs of the WECs for each location.

The annual absorbed energy represents the income side of a wave energy project, by integration of external dimensions, working principle, machinery function and local wave resources. However, this is not a sufficient measure because the critical factor in the feasibility of the project is the average economic cost per kilowatt-hour over the device life span, or life cycle. This requires cost estimation, which is a complex task ([Babarit et al., 2012]). As long as the technical solutions are uncertain or unknown on a detailed level, cost estimates are inevitably hampered by large uncertainties. Adressing this issue is out of the scope of this work. Here, the focus lies on the availability of potential resources and its potential change in a life-cycle along the continental margins.

Deep water installations are not expected to be affected by sea-level rise ([Harrison and Wallace, 2005]), but could be impacted by other factors from a changing climate. [Harrison and Wallace, 2005] carried out a sensitivity study to quantify how changes in wind (and in consequence in wave climate) influence energy production, by using a relationship between wind speed and the Pierson-Moskowitz spectrum. A more detailed investigation is made by [Woolf and Challenor, 2002] using numerical modeling to study the effect of the change in storm frequency, intensity, tracks and propagation speed over the wave heights in the North-East Atlantic.

Two different risk arises when considering offshore WECs and changes occurring in the marine climate. Firstly, risk associated with the structural safety of the installation, usually designed for certain stationary conditions, in an environment of high variability through its life cycle. This dimension of the problem mainly deals with the survivability of the installation.

Secondly, in the operation of a wave-farm, the conditions for which it was originally designed may also change with time, not only the extreme conditions but also the mean or the number of calms sea-states are presumed to change. The degree in which this can occur must be considered and, if possible, quantified.

4.3.2 Methodology: a risk analysis approach

An estimate of the wave energy absorbed by a particular device at a particular location can be obtained by crossing the device power matrix and the scatter diagram of wave statistics (i.e. 2D

histogram). As the resources diagram is available (see previous sections), the problem is reduced to the definition of the the power matrix of the devices. Due to the lack of public information about wave power matrix of prototypes and designs of converters, this work relies on several of the WECs presented in [Babarit et al., 2012] obtained by numerical modeling. This work found good agreement with the limited public available information. The authors used Wave to Wire models to derive the power matrices of each device for several sites in the European North-Atlantic coast. Hereafter, it is assumed that these energy matrices are representative of a typical North-Atlantic energy scatter diagram, represented in Figure 4.25. The location of the point is represented in Figure 4.26, in the North-Atlantic, centered in the area used for the simulation of WECs power matrices in the said work.

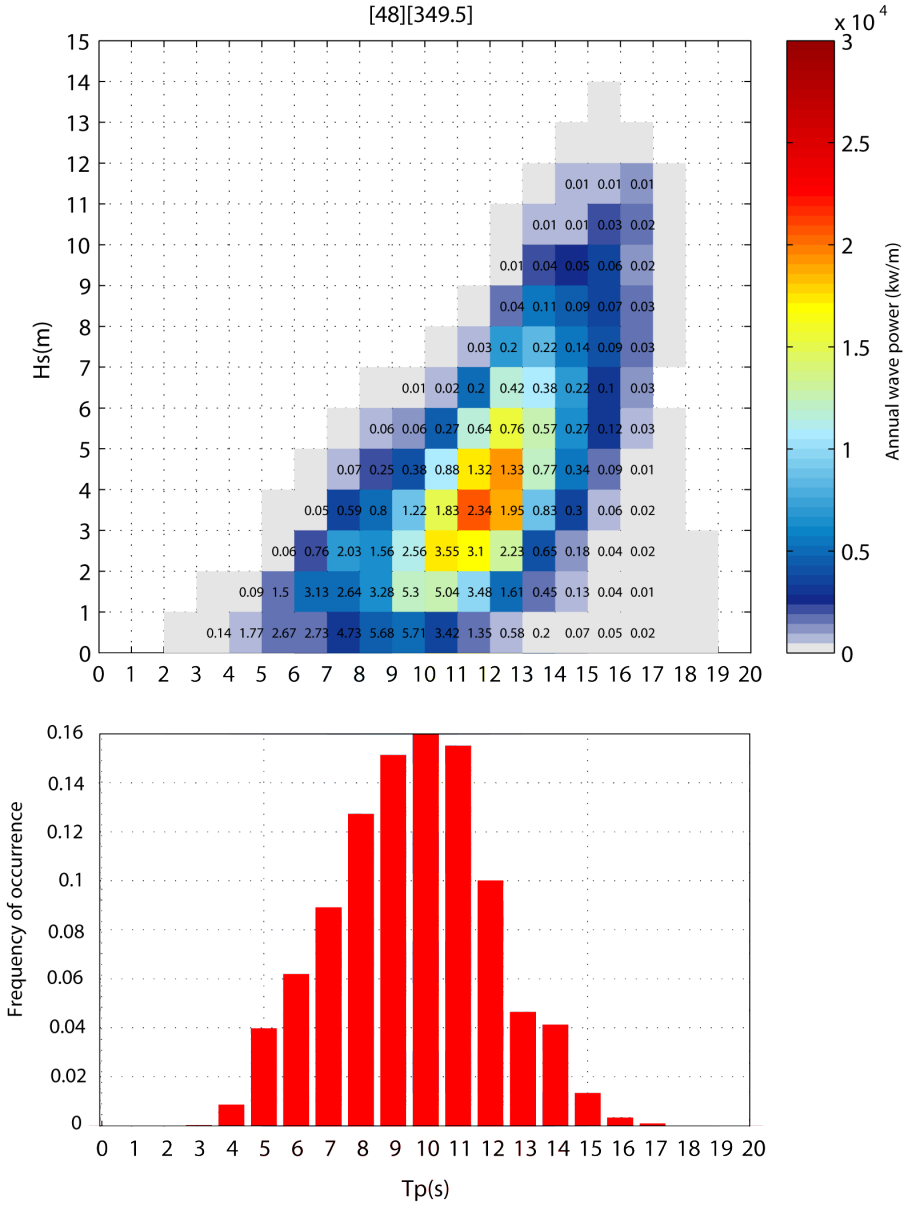

Figure 4.25: Scatter diagrams of wave power (upper panel) and occurrence histogram (lower panel) of a representative point in the North Atlantic. Coordinates: 12°W, 47.8°N.

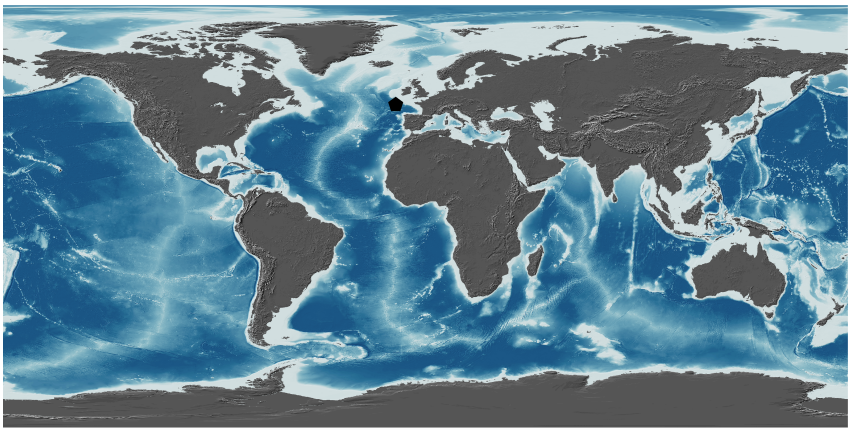

Figure 4.26: Location of point selected for wave energy resources characterization and used as benchmark reference for wave energy converters scaling procedure.

4.3.3 Technological Risk approach

The assessment of technological risk associated with wave farms is based on the global framework of risk analysis described in Chapter 1. However, a modification in the terms of reference is introduced justified by the different nature of the subject. Taking into consideration that global wave power is increasing at the continental margins as a rule (see previous results), the original equation for risk (Chapter 1) is adapted so that the risk is, in this particular case, defined as an Opportunity (O) resulting from the integration of a function of the probability of obtaining a certain production (f_P) and its Revenue (R). Note that the Opportunity and Revenue of a production are equivalent to the Hazard and Consequences terms, respectively, for impact assessments. Expressed in mathematical terms:

$$O_{now} = \int f_P(p) \cdot R(p) dp \tag{4.10}$$

A sketch of this equation is represented in Figure 4.27. Since the production (i.e. probability) depends on more than one variable: wave heights (H) and periods (T); and the Revenue can be expressed as the product of a certain Production (P) and a its corresponding Value (V); the equation adopts the form:

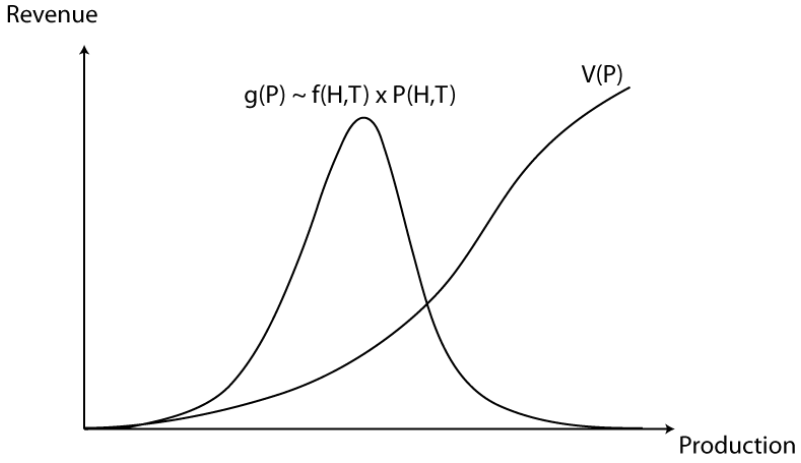

Figure 4.27: Sketch of probability density function of production and revenue function from wave power

$$O_{now} = \int \int_{H,T} f(H,T) \cdot P(H,T) \cdot V(P) dH dT \tag{4.11}$$

where $f(H,T)$ represents the probability density function (pdf) of wave heights and periods, $P(H,T)$ represents the production obtain for each pair of wave heights and periods, and $V(P)$ its value in monetary terms.

This probability density functions can be obtained from historical data. However, the distribution of wave heights and periods is site-specific and the production function from these variables depends on each WEC device.

Note that a simplification can be adopted where the pdf of wave heights and periods, multiplied by its associated production, may be expressed in an aggregated production pdf, denoted as g_P. To assess the Opportunity of exploitation for a future year (O_t), the pdf of production varies (being now $g'_P(p)$ and would be obtained similarly:

$$O_t = \int g'_P(p,t) \cdot V(p,t) dp \tag{4.12}$$

Another difficulty is that the pdf of production for the future ($g'_P(p,t)$) is not known in principle. This can be sorted out by considering stationarity of past changes and assuming the future production as an extrapolation of long-term historical changes for the life cycle of the installation (i.e. few decades). This is sketched in Figure 4.28, where TS represents the time span of data, LC the life cycle, DY the increment in production in the past and dy the expected increment in production for the future from statistical extrapolation. The production time series show a significant long-term trend, computed over 6 decades, that may be extended to the next coming decades (i.e. 30-year Life Cycle) to assess the possible change in production.

If the annual absorbed energy represents the income side of a wave energy project, the value of production, $V(p,t)$, can be assumed to be linear and constant in time, although the methodology allows for any shape that it could adopt. Note that if considered to be linear, the opportunity results when expressed in proportion to actual wave power resources will only represent the change in production and not the elasticity of the revenue curve.

This methodology has been followed in the work for comparison of exploitation conditions in four different devices along a life cycle of 30 years.

The structural design of wave farms is conditioned by the extreme wave heights ([Cruz, 2008]) among other factors. To consider the risk of survival of the infrastructure as a function of change in wave extremes a different approach must be followed.

When dealing with a structure design, the return period is useful in calculating the risk of the structure, given the design life expectation. This is the likelihood of at least one event that exceeds design limits during the expected life of the structure, which complements with the likelihood that no events exceed design limits. The equation for assessing this risk along the installation expected life can be expressed as:

$$R = 1 - [1 - Prob(X >= x_t)]^n = 1 - [1 - \frac{1}{T}]^n \tag{4.13}$$

where $Prob(X >= x_t) = 1/T$ is the probability of the occurrence for the failure event in question and n is the expected life of the structure.

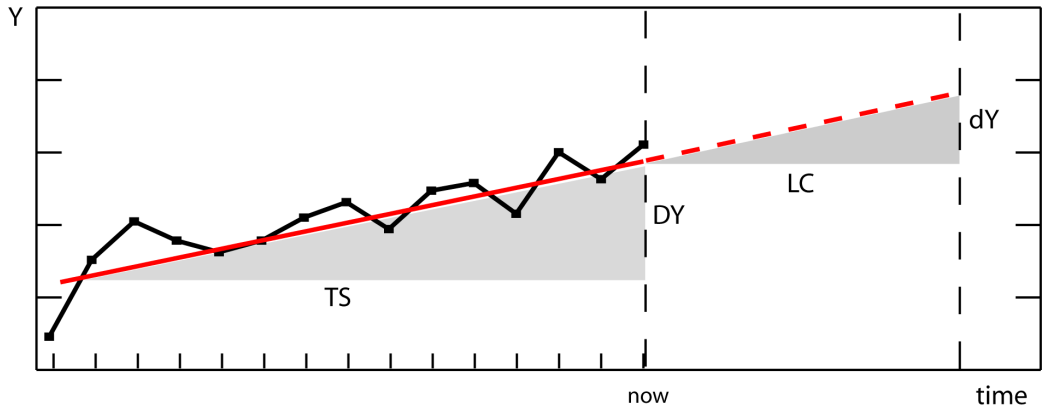

Figure 4.28: Sketch of long-term change in the wave power absorption for a wave energy converter device and extension of rate of change for its life cycle. TS represents the time span of past data, LC the life cycle period, DY the long-term variation during the TS period, and dy the expected change obtained by extrapolation of past changes.

In the former expression no considerations on consequences of failure are incorporated to the risk computation. It is assumed that the failure of the installation is reached if the failure event occurs, which is not completely true. Reparation damage could be incorporated for a more realistic study but it will also require a simulation approach for life-cycle analysis.

Note that the risk of failure for a certain year is 1-1/T(t), assuming that the return period can vary with time. This implies that the variation in the risk of failure of the installation at the start and end of life cycle is indicated by the ratio between both return periods, as:

$$\delta R = 1 - \frac{T(t = LC)}{T(t = 0)} \tag{4.14}$$

where LC represents the time at the end of the life cycle period. This expression has been used for the comparison of the risk of failure at the start and end of the installation operations period.

4.3.4 Wave Energy Converters considered in the analysis

This work intends to contribute to clarify what can be reasonably expected as the mean output of several devices along the world coastline. The devices on which this work is based are provided in [Babarit et al., 2012] by numerical simulation and only those four suitable for deep waters are compared. The geometry and configuration of each device were inspired by well-known WECs currently under development by different technology companies. It should however be noted that there can exist significant differences in geometry and configuration with the original power matrices.

The main objectives are: (1) to compare the installation of four devices accounting for actual

wave energy, and (2) define which device is expected to be less affected by variations in the wave resources along its life cycle due to long-term climate changes. Owing to the numerous assumptions and the lack of information along the process, this work can be considered as a suggested measure of wave absorption and a methodology for comparing devices. With more accurate information of the technologies and the optimum design of devices for different wave climates more realistic results could be obtained.

More details about the simulation and device information can be obtained in [Babarit et al., 2012]. For a review of technologies and working principles, [Falcao, 2010] can be consulted. The devices used herein are described below:

- Floating two-body heaving converter (F2HB):

  This device is inspired by the Wavebob WEC currently under development in Ireland. It is an axi-symmetric, self-reacting point absorber, operating in the heave mode. It is composed of a torus sliding along a vertical float. The hydraulic power take off system is driven by the relative motion between the two bodies. The characteristic mass of the device is estimated about 5,700 t and the wetted surface area about 2,100 m^2.

- Floating oscillating water column (FOWC):

  This device, inspired by the OE buoy, developed by Ocean Energy Ltd. in Ireland, is a particular type of oscillating water column device known as the backward bent duct buoy. It has a single air chamber and is free to move in six degrees of freedom. The water column inlet is on the downstream side of the device. The power conversion is provided by an air turbine connected to an electric generator. The motion of the water column relative to the oscillating body creates oscillating pressure in the chamber and air flow through the turbine. The characteristic surface area is about 6,500 m^2 and the characteristic mass of 1,800 t.

- Floating three-body oscillating flap device (F3OF):

  This device is inspired by the Langlee WEC, under development in Norway. It consists of four hinged flaps all connected to the same frame. The relative motion between each flap and the main frame is converted into useful energy. The characteristic mass of the whole original structure is estimated to be about 1,600 t and the characteristic surface area about 2,200 m^2.

- Floating heave-buoy array (FHBA):

  This system is a multibody floating device, composed of many heaving buoys connected to a common submerged reference structure. The support structure is connected to ballasts baskets through tension wires. The total buoyancy force from the buoys is balanced by net gravity forces of the bridge and the ballasts. The buoys are connected to the submerged structure via a hydraulic power take off system converting the energy. The characteristic surface area of the original design is about 4,700 m^2 with a characteristic mass of 5,200 t.

The power matrices of each device have been used to account for the absorbed wave power in a point in the North-Atlantic (shown in Figure 4.26), centered in the region where the different

F2HB	FOWC	F3OF	FHBA
86.52	85.79	86.53	85.10

Table 4.3: Percentage of wave power within the limits of WEC wave power matrices

devices were designed for. These power matrices present ranges in wave heights and periods for exploitability, as no all sea-states are exploitable. Taking this into account, Table 4.3 shows the percentage of wave power, relative to the potential wave energy, taken into account by the boundary mask of each device. The four device here considered could exploit theoretically in the region of 85% of the potential resources. The actual absorption would be lower since not all the wave energy can be absorbed.

Assuming that the design of the different WECs can be optimized for each wave climate type, by modifying its dimensions and configuration, a scaling of the power matrices must be carried out prior to estimate the energy absorption for other locations. This issue is addressed in the next section.

4.3.4.1 Scaling of wave energy converters

The Froude number is the dimensionless quantity $U/\sqrt{g \cdot L}$, where U is a characteristic velocity of flow, g is the acceleration of gravity, and L is a characteristic length. The Froude number can be interpreted as the ratio of the inertial to gravity forces in a flow. In fluid mechanics, the Froude number is used to determine the resistance of a partially submerged object moving through water, and allows the comparison of objects of different sizes. In free-surface flows (e.g. rivers, wave motion), gravity effects are predominant and the model-prototype similarity is performed with a Froude similitude as:

$$Fr_1 = Fr_2 \tag{4.15}$$

If the gravity acceleration is the same in both the model and prototype, and λ represents the geometrical similarity scale ($\lambda = L_1/L_2$), a Froude number modeling implies:

$$V_1/V2 = \sqrt{\lambda} \tag{4.16}$$

$$T_1/T2 = \sqrt{\lambda} = \lambda_T \tag{4.17}$$

and

$$WP_1/WP_2 = \lambda^{(5/2)} \tag{4.18}$$

so that the time is scaled with $\sqrt{\lambda}$ and the wave power scales with $\lambda^{(5/2)}$.

Based on this dynamic scaling, the shape of the power matrices, specifically designed for the North-Atlantic, are transferred to other wave climates in the global ocean. This scaling implies

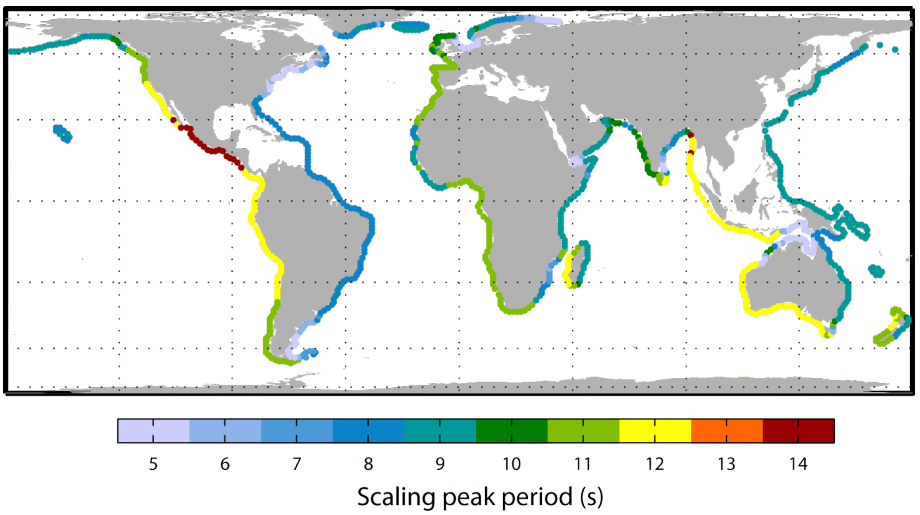

Figure 4.29: Representative periods for scaling of power matrices.

that a wave energy converter can be optimally designed for different wave climate conditions (i.e. different wave power diagrams) and the main variable that defines the design scale is the representative wave period.

The location of the point used as reference for the scaling of the power matrices is shown in Figure 4.26. Changes in power matrices mainly depend on the wave periods rather than on the total wave power. Although there exists a great variability along the North-Atlantic coastal margin in terms of wave power (see previous sections), it can be assumed that the variability is lower for wave periods and so the scaling varies smoothly along the different points as can be seen in Figures 4.29 and 4.31. Therefore, the peak period taken as reference for scaling has been the period with highest absolute frequency, which statistically coincide with the mode of the periods.

The representative period to define the scale for each site has been selected as the most representative of the wave climate at each location. It has been defined as the statistical mode of the periods histograms or, alternatively, the most probable period, should it be higher than the mode. The scale for periods is therefore defined by:

$$\lambda_T = \frac{T_{site-representative}}{T_{reference-Atlantic}} \tag{4.19}$$

The representative periods of wave climate to define the scale are shown in Figure 4.29.

The eastern margin of the Pacific presents the largest periods, 12 s and reaching 14 s in the tropical region, while the western Pacific is in the region of 9 s. The Atlantic Ocean has representative wave periods between 7 and 8 s for the western margin and larger in the east, between 9 and 11 s. The Indian Ocean generates wave periods of 12 s in the eastern continental margin; at the northern and western border they are about 9 and 10 s. This spatial variability is much related with the wave periods climatology seen in Chapter 3.

Figure 4.30 shows the difference between the representative period (Figure 4.29) and the periods that present a frequency of occurrence below 0.2%, that can be considered to be unusual. This value express the range of variation of wave periods and therefore constitutes an indicator of sea-states out of the reach of the wave power optimum design.

The results indicate that the largest variation occurs in the tropical eastern coast in the Pacific, with over 12 s of range, followed by the Indian Ocean, especially the northern coast, with a range of variation of about 10 s. The rest of the continental margins remain in the region of 6 s of difference, being slightly larger, of about 8 s for the eastern Atlantic margin and high latitude regions.

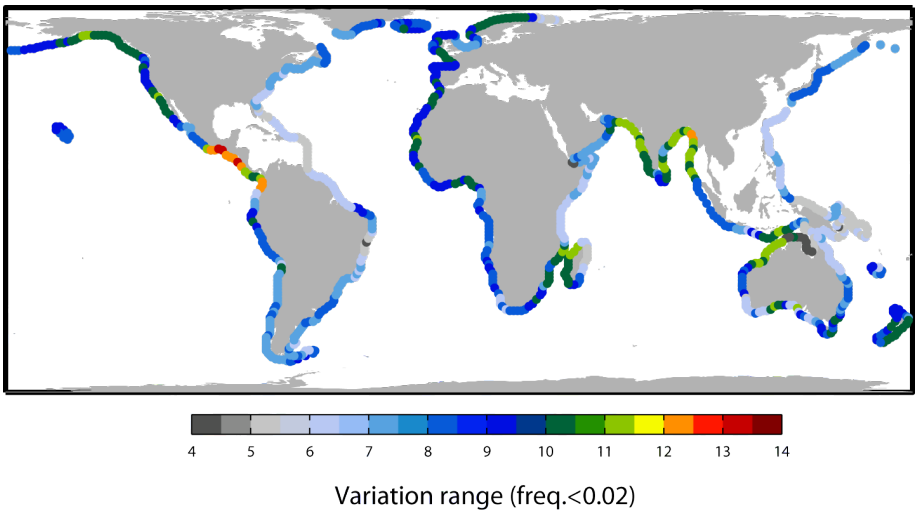

Figure 4.30: Range of variation of period distribution. Limits of the range have been selected as those periods with over 2% of frequency of occurrence.

Assuming a representative period of 10 s from the characteristic wave climate in the northern Atlantic, where the four devices were designed specifically for, and considering the representative periods as a function of wave climate (Figure 4.29), the corresponding scales for periods and dimensions are displayed in Figures 4.31 and 4.32, respectively. As a general rule, the eastern margins of the oceans present no scaling (i.e. $\lambda_T = 1$) while the western margins are affected by a scale for periods between 0.8 and 0.9, in agreement with conclusions in Chapter 3 on wave periods climatology. Some areas that are protected from ocean swells (e.g. Northern Sea or Flores Sea) would need a lower scaling, below 0.5 for periods. Obviously, as the spatial scale depends on the square of the periods scale (see equation 4.17), the reduction in the dimensions will be higher as shown in Figure 4.32.

An example of scaled matrices, along with the original power matrix (upper panel) considered for each device are shown in Figure 4.33. It can be clearly seen how the power matrix is reduced for wave climates with a representative period (9 s for point 4; see Figure 4.29) lower than the reference period (10 s, taken as reference for the device design) and increased for larger representative periods (12 s for point 9).

Note that this approach is producing some error as the wave power matrices do not cover

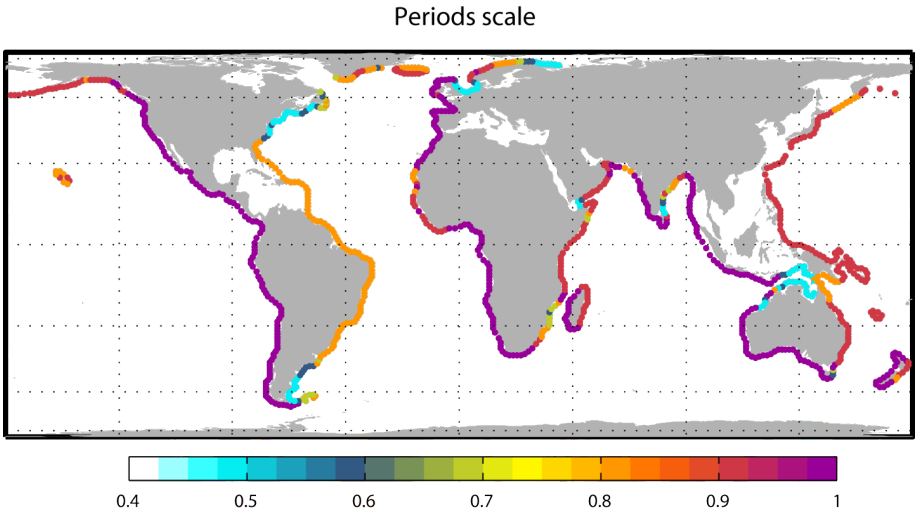

Figure 4.31: Periods scale.

the full range of sea-states occurring (see Table 4.3). The percentage of Incounted Wave Power (IWP), in kwh of absorbed energy, which discounts sea-states where absorption is out of range, can be computed from:

$$IWP = \frac{\sum HWP(t)}{\sum PWP(t)} = \frac{\sum_{T_p} \sum_{H_s} WP_{WEC}(i,j) \cdot N(i,j)}{\sum_{T_p} \sum_{H_s} WP(i,j) \cdot N(i,j)} \tag{4.20}$$

where HWP represents the harvested wave power, PWP the potential wave power, N(i,j) the number of occurrences of sea-states with parameters (i,j), WP the total potential resources and WP_{WEC} the potential resources that lies within a certain boundary (delimited by a mask) of the total potential resources:

$$WP_{WEC}(i,j) = WP(i,j) \cdot mask(i,j) \tag{4.21}$$

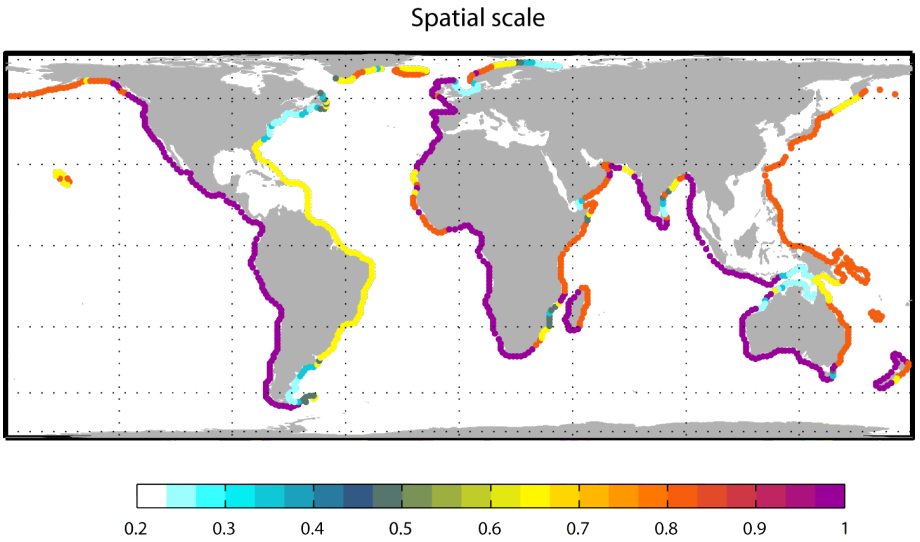

Figure 4.32: Spatial scale.

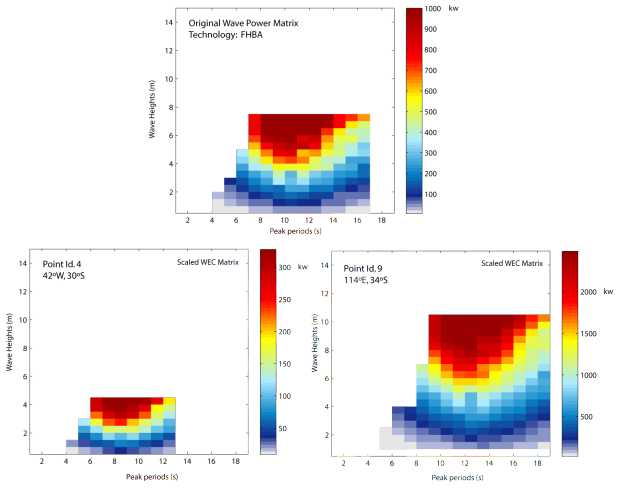

Figure 4.33: Example of FHBA dynamically scaled power matrix at two representative locations.

4.3.5 Performance at design age: comparison of devices

The IWP is used herein (see Figure 4.34) as an indicator of the absorbed wave energy of the scaled devices along the continental margins. Alongside with this indicator, the annual HWP is also considered for the comparison since it represents the potential wave power that each device may absorb, considering their particular range of wave heights and periods, per unit of wave length. The HWP is represented in Figure 4.35.

Despite the absorption range of each device, the performance to absorb wave energy is crucial for comparison. The annual absorbed wave power (in Twh/yr) for each device is represented in Figure 4.36 showing different optimum regions for each device. This information has been aggregated along continental regions in Table 4.4 as an indicator of performance for each device.

The main conclusions arisen from the resources availability and the absorption range for each device follow:

- One aspect that should be emphasized is the considerable proportion of the wave power considered in the power matrices range (incount mask) of each device, according to the IWP index. Approximately all devices cover the same proportion of potential resources, in global terms (Table 4.3) and also spatially after the scaling process (Figure 4.34).
- With respect to the HWP, this means, not considering the proportion but the wave power covered by the range of exploitation for each device, all devices show a similar performance, as seen for the IWP index (Figure 4.34). F3OF seems to show the worst spatial performance in the SH though.
- If the proportion of resources covered for each device is similar, the annual absorbed wave power (Figure 4.36) is a fair variable to measure each device performance and, also, it allows their comparison. FOWC and FHBA devices boast the best performance in both hemispheres. Particularly worth mentioning are their absorption at high latitudes in the SH and at North-Atlantic and North-Pacific basins, reflecting an adequate behavior for rough conditions. FHBA additionally reveals itself as a particularly good technology for clean swell conditions judging by its performance in the Guinean Gulf (T=10 to 11 s) and in the western Atlantic (T=8s). On the contrary, F3OF seems to behave very poorly at mid-latitudes and at western Pacific.
- Using any of this technological solutions at all the points of study, approximately a total of 140 Mwh/yr could be harvested. This value does not account for technological or other losses, nor does it count for the dimension of the wave farm with respect to the device dimensions (i.e. more than one device can be installed at each location analyzed). The analysis only aims to compare the devices and therefore the 140 Mwh/yr can not be compared with the 3 Twh/yr estimated as the potential wave resources available. Including the consideration of the density and number of devices per surface of wave farm would address this issue but it is out of the scope of this work.
- This last point seems to be borne out by a rather surprising fact: in Table 4.4 the highest absorbed wave power corresponds to the F3OF device. This is explained by a higher absorption at highly rough-open areas like the northern Atlantic and southern Ocean that

compensate the aggregation values for each continental region. As a conclusion, this technology would be adequate specifically for very rough conditions while it underperforms at smoother conditions, as seen in the spatial representation.

- The analysis further reinforces the need for a site-specific study of each device, although the general conclusions and the methodology for comparison may provide useful guidance.

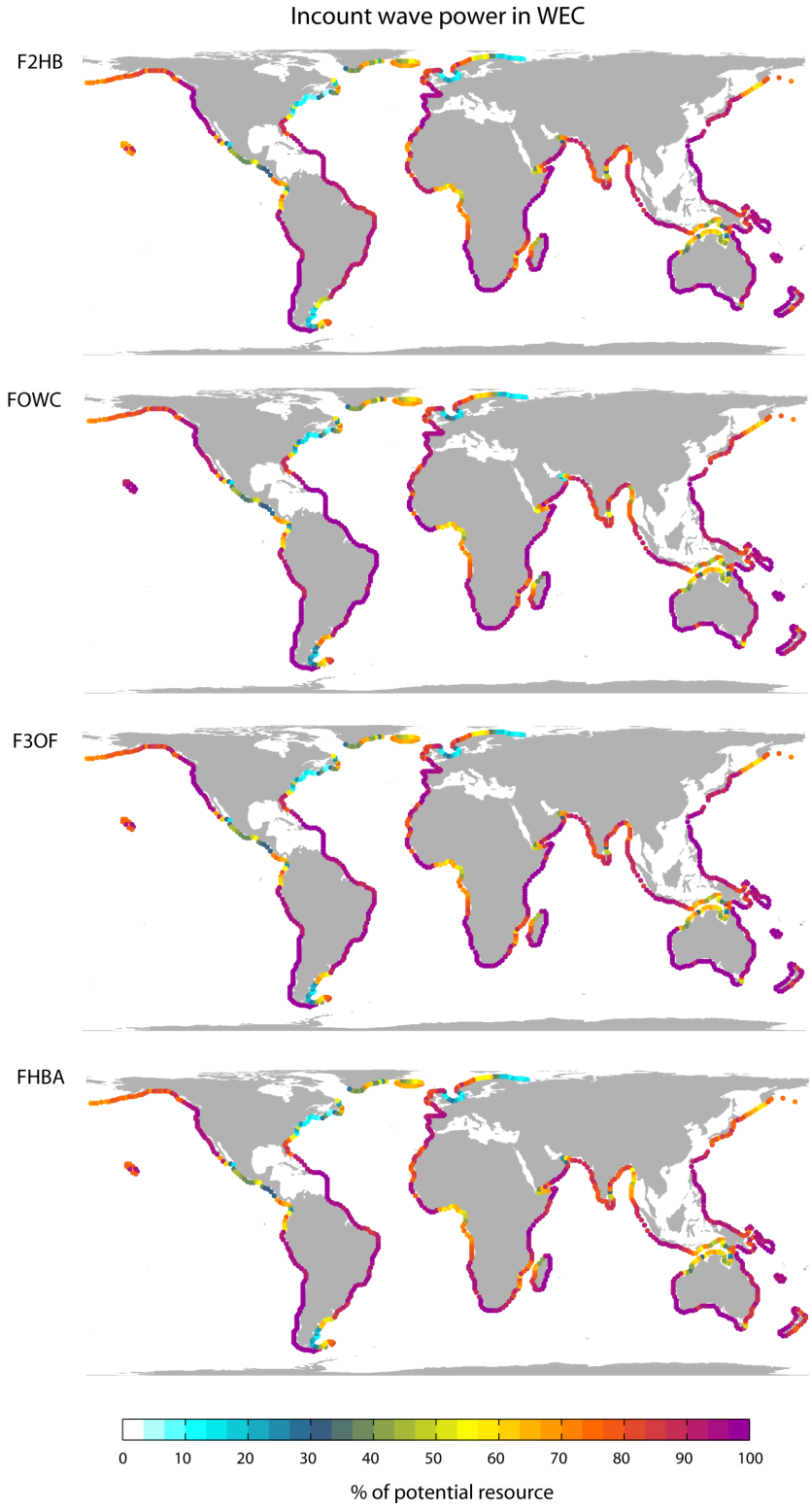

Figure 4.34: Incount Wave Power (IWP) index representing the proportion of potential wave power (%) covered by the range of possible periods and heights for each device.

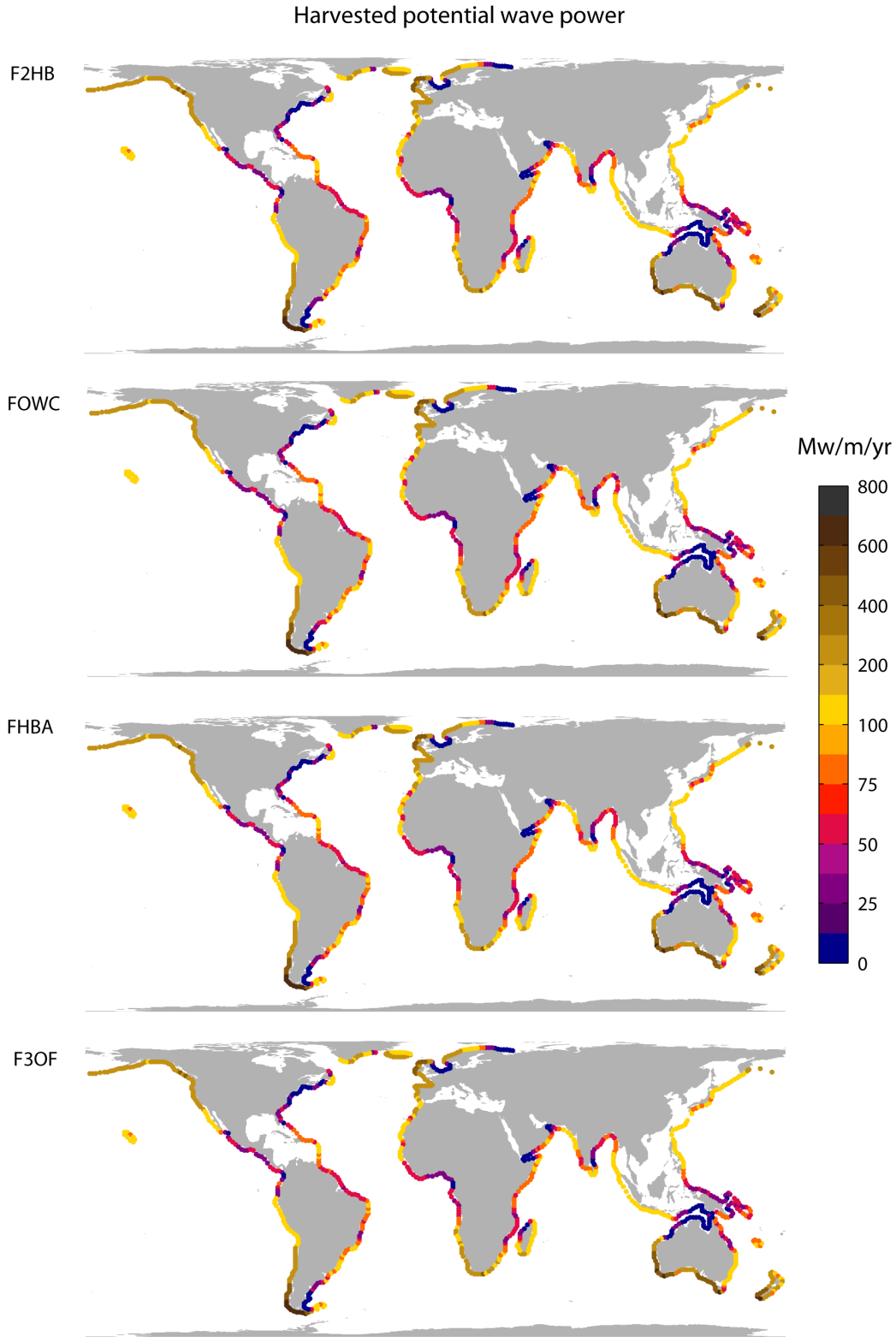

Figure 4.35: Harvested annual potential wave power for each device depending on the range of absorbing wave heights and periods (Mw/m/yr).

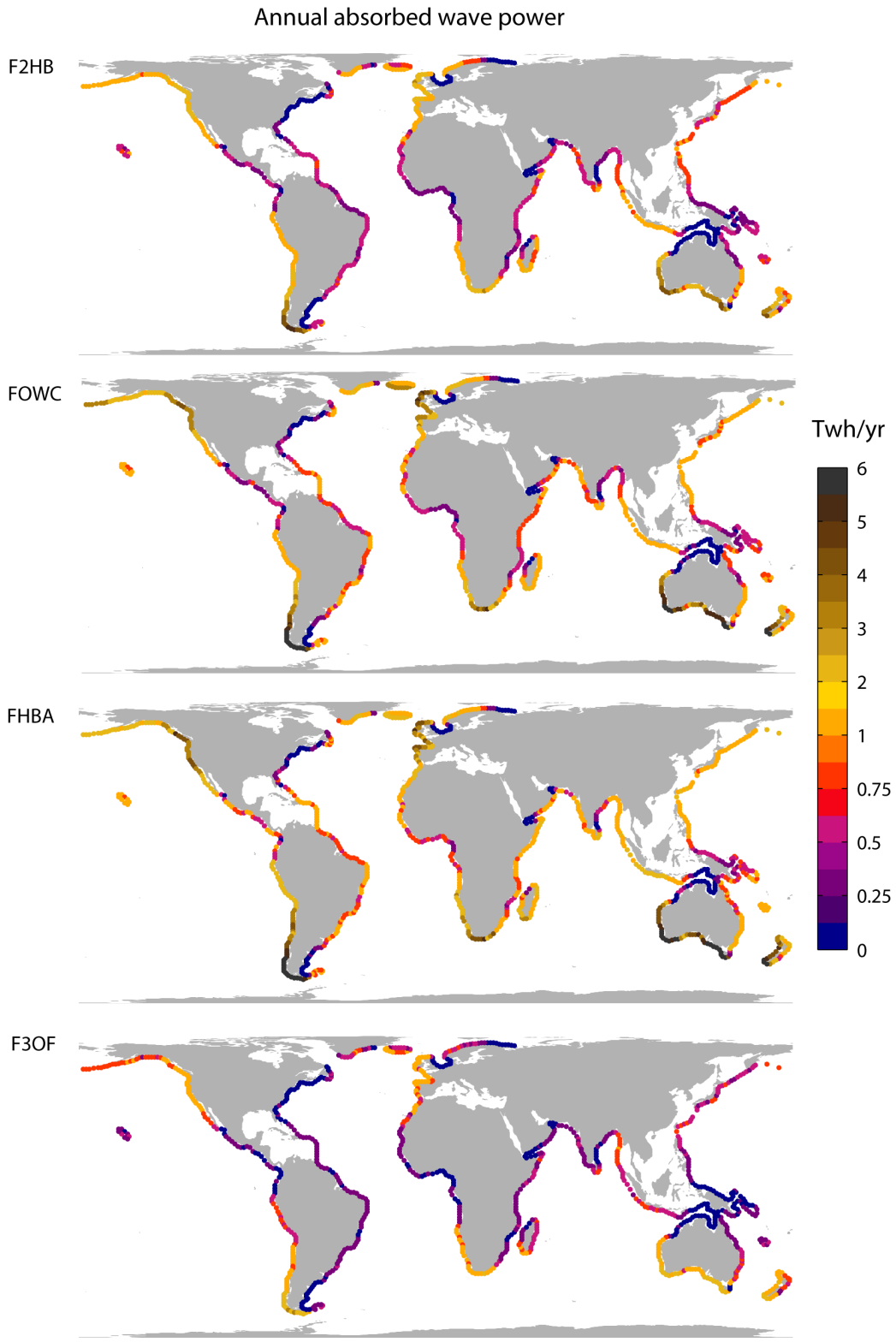

Figure 4.36: Annual total absorbed wave power for each device (Twh/yr).

	Wave Energy Converters			
REGION	F2HB	FOWC	F3OF	FHBA
North America (W)	17.53	17.49	17.70	17.21
North America (E)	3.93	4.18	4.06	4.00
South America (W)	19.51	19.43	19.52	19.36
South America (E)	6.98	7.41	7.20	7.05
Hawaii	1.20	1.52	1.32	1.32
Greenland and Iceland	7.51	7.62	7.60	7.36
Europe (W&N)	15.65	15.86	15.85	15.55
Africa (W)	9.49	9.60	9.65	9.34
Africa (E)	5.71	5.76	5.76	5.55
Madagascar	3.63	3.58	3.66	3.55
Asia (S)	5.74	5.54	5.80	5.41
Polynesia	6.59	6.54	6.62	6.53
Asia (E)	7.06	6.94	7.09	6.74
Australia and New Zealand	28.32	27.89	28.40	27.42
GLOBAL	138.85	139.36	140.25	136.39

Table 4.4: Global and regional absorbed wave power (in Mwh/yr) for each device.

4.3.6 Performance at the end of device life cycle

The wave power has been varying in the long-term during the last decades as has been previously shown in Section 4.2.3. Without losing light of the fact that the life cycle of WEC installations rarely would exceed 30 or 40 years due to amortization, maintenance conditions and outdating of technologies, among other numerous factors, a future wave power that follows (in average) the current rates of change might be expected for the next coming decades. Considering the absorption ranges and the different performances for each device, for a common long-term change, a distinct effect may also be expected for each technology. To explore this issue, the time series of annual absorbed wave power have been analyzed for each device and the long-term trends computed. Results are shown in Figure 4.38. Figure 4.37 includes also the past changes in the potential resources as a benchmark for comparison. The percentage of change, defined as the past change relative to the absorbed wave power for each device, may be a better indicator of the technological risk for each technology. The performance is expressed in Figure 4.39 in such a manner.

The main conclusions arisen from the expected change in the absorption for each device are:

- Comparing with the past changes in potential wave power, FOWC technology exhibits the greater changes, while F3OF displays an opposite effect being the change negligible in magnitude.
- F3OF is generally the less affected technology.
- F2HB, FOWC and FHBA all show an increase in the eastern Pacific margin, that does not appear in the potential resources.
- FOWC is very sensitive to changes in the SH.
- In the North-Atlantic conditions, the area for which the devices were originally designed, all technologies show a good performance. This is probably because the trends in wave

power (along with the rest of wave climatic variables) are weaker than in other regions of the globe.

- A general positive increase is found for all devices with a singular exception at tropical latitudes for F3OF technology. F3OF seems to be more affected in proportional terms, indicating a lower reduction in those areas as stated in the previous point. A clear reduction of absorption stands out at mid Atlantic and bay of Bengal as singular points. A similar opportunity for increased production is identified for FHBA, although not that clear.
- All devices would experience a reduction about -10% in the south-west Pacific (Philippines to Papua).
- F3OF and FHBA are less sensitive to changes in the SH, proportionally speaking.
- In any case, the highest opportunity (both in proportion and in magnitude) takes place along the Pacific coast of central America.
- Different performances for each device are further confirmed.

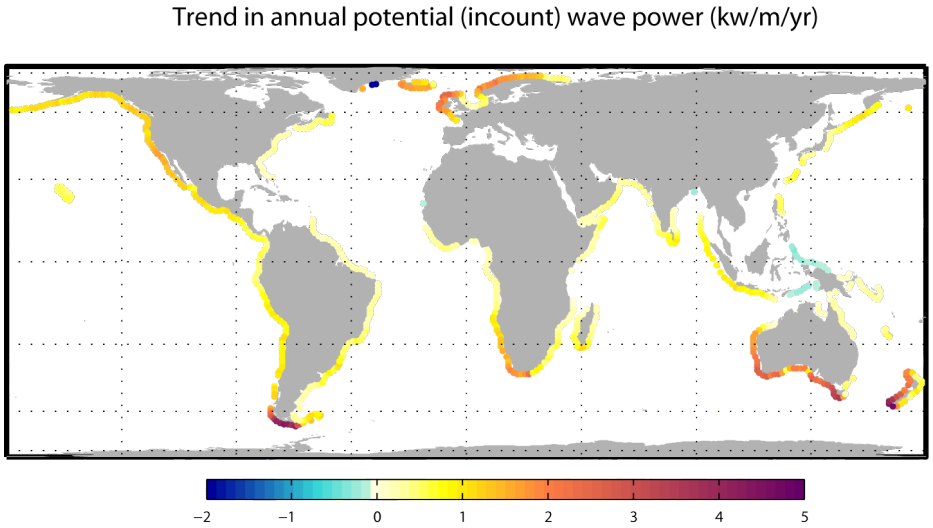

Figure 4.37: Long-term trend in the potential wave energy resources.

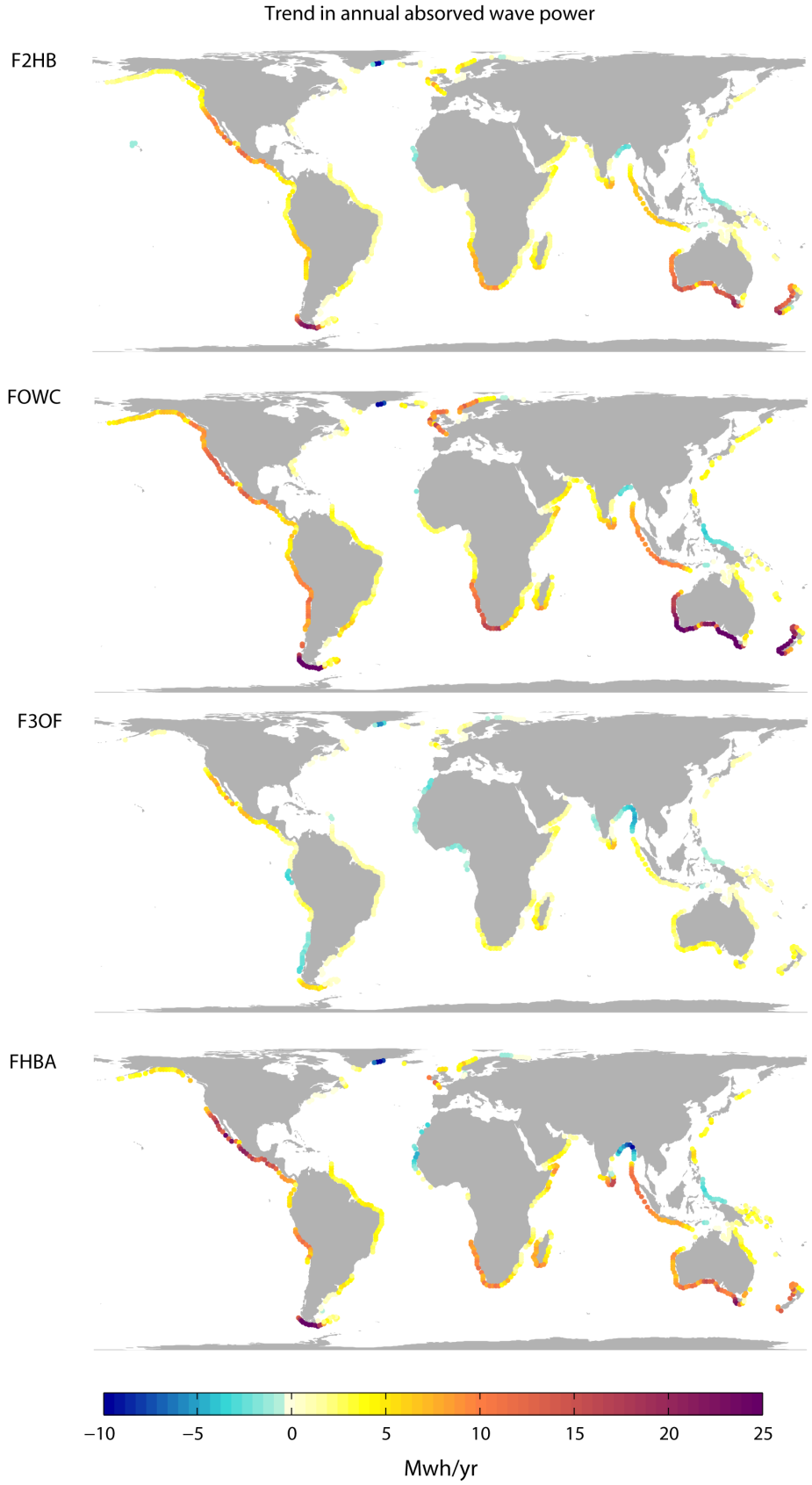

Figure 4.38: Long-term trend in the absorbed wave power for each device.

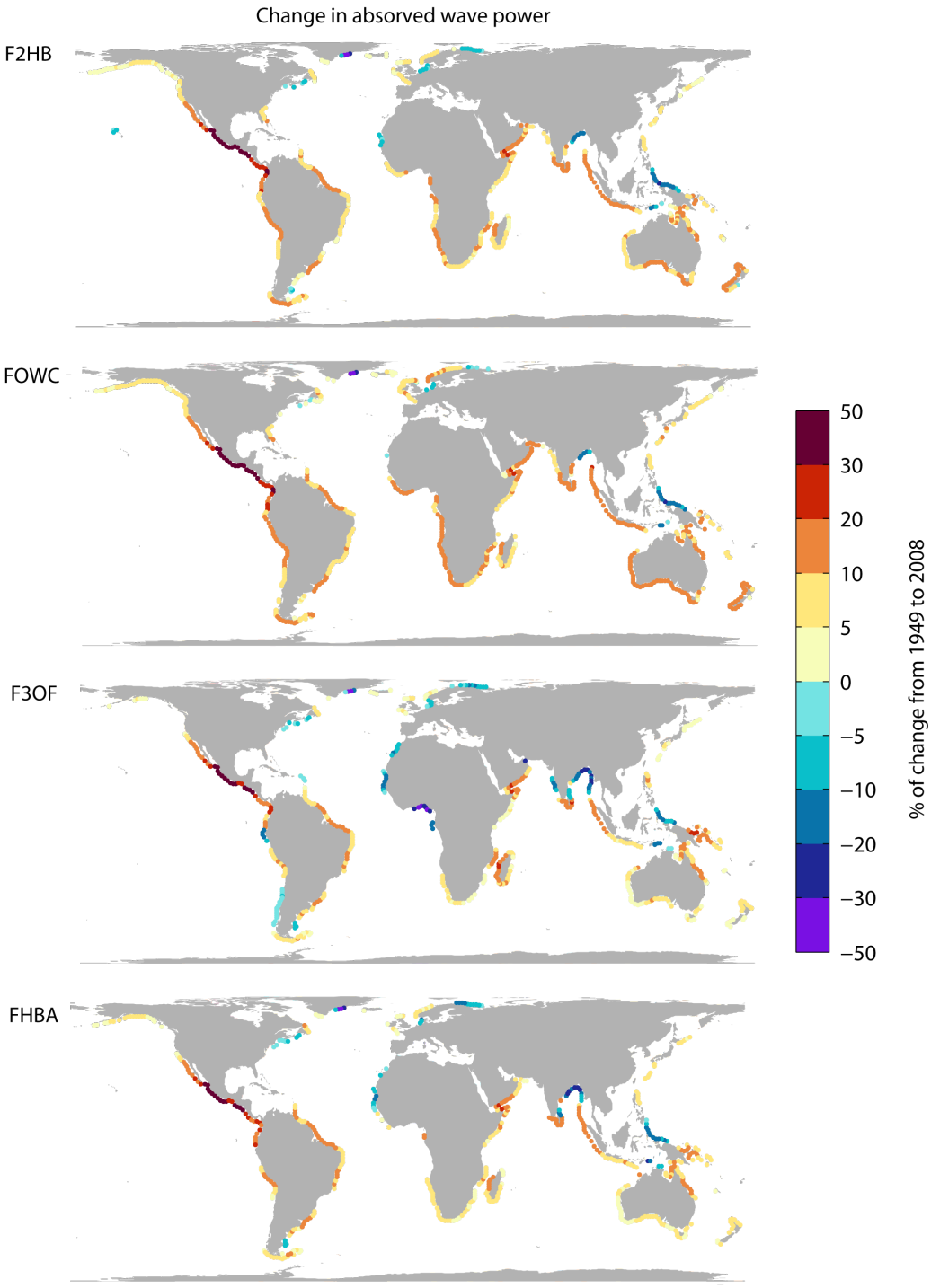

Figure 4.39: Percentage of change of the absorbed wave power with respect to the mean absorbed wave power for each device.

It must be remarked that these results are only an approximation since they rely on the analysis of absorbed wave energy time series. A more accurate analysis would express the changes in the wave heights-periods distribution, i.e. how the histograms of occurrence may change along the life cycle of the installation. Specific and optimum design power matrices would also be necessary for a fair comparison of technologies before taking an installation decision.

4.4 Survival risk

As explained previously, the structural design of the installation are conditioned by the most extreme wave events. The 100-year significant wave height is usually used as an indicator of the structural design cost ([Cruz, 2008]). As seen in Chapter 3, devoted to the global wave climatology, return period of wave extremes are varying (see Figure 3.30) and the range of variation in the life cycle should be considered.

The proportion of safety can be determined from the ratio of the initial probability of failure at the design age and at the end of the life cycle:

$$SI = (1 - \frac{T(t = LC)}{T(t = 0)}) \cdot 100 = (1 - \frac{T(t = LC)}{100}) \cdot 100 \tag{4.22}$$

This index, defined as Security Index (SI), is a representative indicator of the risk for the installation survival, assuming total failure if the event associated with 100-yr return period is reached. Figure 4.40 represents this index. Negative values of the index are indicating a decrease in the return period for the wave events associated with today's 100-yr return period. As it can be seen, the reduction in safety is generalized with scattered exceptions. Most affected areas would be low latitudes of eastern Pacific, high latitudes in south-America, southern part of Africa and north-western Pacific.

It is without doubt that survivability of devices would depend on many other factors like weight, size or structural configuration. These issues are, however, out of the scope of the present study and require more detailed information on devices.

4.5 Conclusions

This chapter builds on a global wave reanalysis (GOW) to perform two main tasks: (1) evaluation of the global wave energy resources, describing its spatial-temporal variability throughout different scales; and (2) a risk analysis of absorbed wave power for four offshore Wave Energy Converters (WECs) with a twofold scope: resources change in a life-cycle and survivability risk from expected variations in the 100-yr wave height.

For the evaluation of the global wave energy resources, the GOW database was validated with buoy data in wave power levels for monthly and yearly scales, showing a good agreement at both time scales. The correction applied to the numerical hindcast was also checked in terms

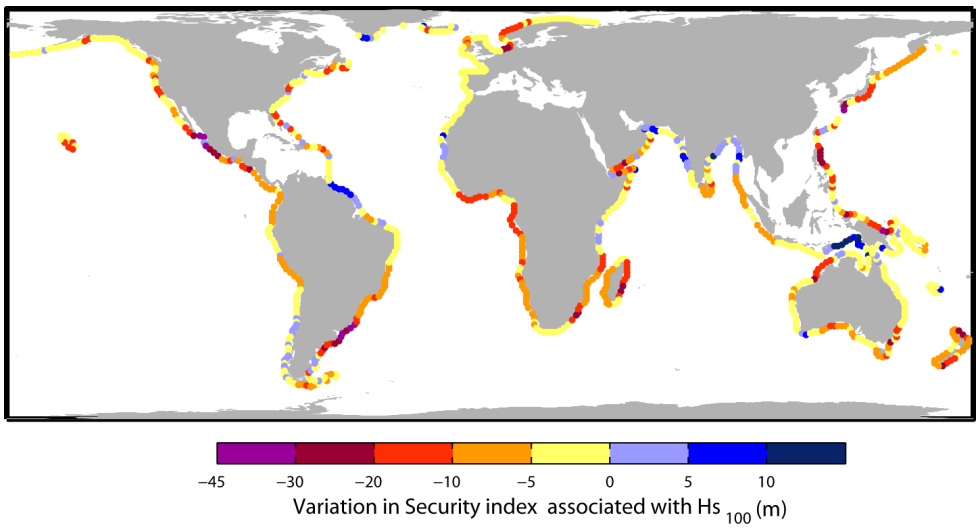

Figure 4.40: Safety proportion at the end of the life cycle of a wave farm taking into account the wave extremes long-term changes.

of wave energy calculation estimates, revealing a considerable correction (over 40%) along the continental margins.

The global offshore wave power is estimated in the range of 1 to 10 Twh (between 9,000 and 90,000 Twh/yr). A recent estimation was made in 32,000 Twh/yr considering all possible directions. In this work a new approach is developed, through a computation of the resources on a hourly basis in the period from 1948 to 2008 and only taking into consideration the transverse directions onshore. The global gross theoretical wave power is hence estimated approximately in 16,000 Twh/yr (corresponding with 1.8 Twh power), being the standard deviation over 1,000 Twh/yr and the mean rate of long-term change of about 58 Twh/yr. This figure differs from previous estimations although when considering the full range of directions the figures are in close agreement with previous works. Only about a fraction of a 25 % of the theoretical resource is roughly considered as an indicator of possible technical absorption in the final converters.

With respect to the spatial variability, the Southern Hemisphere shows a larger resource alongside with a lower variability. Meanwhile, the North-Atlantic, despite its large mean resource, shows a large variance within the year. In general, the Northern Hemisphere presents a larger variability at high latitudes. Tropical areas are, however more stable and, therefore provide a small but sustained resource throughout the year of 15 to 20 kw/m. In other regions of the globe, this variability is also a matter for consideration for design and planning of wave farms. On a regional basis, it has also been detected that the western borders of continents present greater potential and higher variability.

From the correlation patterns with the most prominent climate indices, the most outstanding results are obtained for the AO, NAO, EA and PNA climate indices in the Northern Hemisphere and SAM and SOI indices in the Southern Hemisphere. Although the effect of a climate index on the wave power is larger in magnitude when the available resources are high (winter season), it has been obtained that during the summer months, when the wave climate is milder, the presence

of a certain climate pattern affects at a higher degree. However, in the North Indian Ocean, a region with strong annual variability in the resources, the effect of climate patterns is significantly remarkable in winter, when the variability range is larger. In the light of these results, it has also been confirmed that natural variability is a greater factor to consider in wave energy exploitation and design issues. Moreover, in some cases (like shown in the Southern Hemisphere for the SAM index) inter-annual variability has appeared to be of the order of magnitude of mean seasonality.

Long-term trends have been found in this work. Specially remarkable are the trends found in the Southern Hemisphere, in the region of 1 kw/m/yr and sustained throughout the seasons. However, special caution must be taken regarding the fact that this area of the globe is the less reliable for numerical atmospheric reanalysis, so it is for the wave reanalysis used in the analysis.

Variability of wave power scatter diagrams and frequency of occurrence of combinations of wave heights and periods confirm and support the need for site-specific design of converters for each region of the continental margins.

With the aim of contributing to clarify what can be reasonably expected from several technologies at offshore depths, a risk-based method was proposed to consider the variability of the resources and the long-term changes coupled with theoretical optimal designs of four offshore floating WECs. The risks for wave energy harvesting and the survivability degree of the installation were performed through a life-cycle. Scaling of the four devices was based on Froude similitude so as each wave power matrix was transferred to different wave climate types along the planetary coast. About 85 % of theoretical wave power resource lied in the boundary of absorption (from combination of wave heights and periods) for all devices assuming the scaling procedure. Different behaviors were identified at different latitudes depending on the technology. The results, although a first estimate, demonstrate that different devices are prone to show different performance depending on the wave climate types at different locations. Site-specific optimized design and comparison of technologies is a must for installation analysis.

The trends in the absorbed wave power time series were identified for each device. Should the past changes persist into the future, the different technologies would not show the same respond, being some of them more affected than others. For a more correct assessment, this analysis should be extended to the study of changes in the combination of wave heights and periods, provided that these changes were somehow integrated here in terms of the total absorbed wave power.

Although varying spatially, the results for survival risk, based on the expected changes in the 100-yr significant wave height event, show a generalized reduction of the herein defined security index (i.e. increase in risk). This indicator could be closely related to the design factors for possible future wave farms facilities.